AD-A137 060 THREE DIMENSIONAL/BOUNDARY LAYER INTERACTION: LAMINAR AND TURBULENT BEHAV..(U) VON KARMAN INST FOR FLUID DYNAMICS RHODE-SAINT-GENESE (BELGIU..

UNCLASSIFIED J J GINOUX ET AL. 15 DEC 82 VKI-CR-1983-05 F/G 20/4 NL

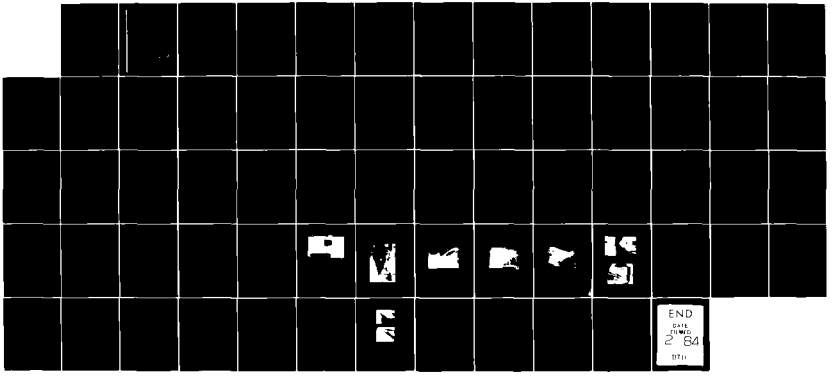

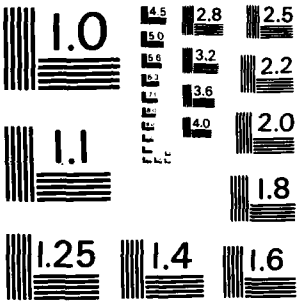

AFOSR-TR- 83-1321

GRANT AFOSR-82-0051

THREE DIMENSIONAL/BOUNDARY LAYER INTERACTION : LAMINAR AND TURBULENT BEHAVIOUR

J.J. GINOUX AND G. DEGREZ

VON KARMAN INSTITUTE FOR FLUID DYNAMICS
CHAUSSÉE DE WATERLOO, 72
B - 1640 RHODE SAINT GENÈSE, BELGIUM

DECEMBER 15, 1982

FINAL SCIENTIFIC REPORT, 1 DEC 1981 - 30 NOV 1982

PREPARED FOR

AFOSR/PKN BOLLING AFB DC 20332

AND

EUROPEAN OFFICE OF AEROSPACE RESEARCH AND DEVELOPMENT
LONDON, UK

SECURITY CLASSIFICATION OF THIS PAGE (When Data Entered)

UNCLASSIFIED

REPORT DOCUMENTATION PAGE

READ INSTRUCTIONS BEFORE COMPLETING FORM

1. REPORT NUMBER: AFOSR-TR- 83-1321	2. GOVT ACCESSION NO.: AD-A127060
3. RECIPIENT'S CATALOG NUMBER:	
4. TITLE (and Subtitle): THREE DIMENSIONAL/BOUNDARY LAYER INTERACTION : LAMINAR AND TURBULENT BEHAVIOUR	5. TYPE OF REPORT & PERIOD COVERED: Final Scientific Report 1 Dec 81 - 30 Nov 82
	6. PERFORMING ORG. REPORT NUMBER: VKI CR 1983-05
7. AUTHOR(s): J.J. Ginoux and G. Degrez	8. CONTRACT OR GRANT NUMBER(s): AFOSR-82-0051
9. PERFORMING ORGANIZATION NAME AND ADDRESS: von Karman Institute for Fluid Dynamics, Chaussée de Waterloo, 72, B-1640 Rhode Saint Genèse, Belgium	10. PROGRAM ELEMENT, PROJECT, TASK AREA & WORK UNIT NUMBERS: 61102 F, 2307/K1
11. CONTROLLING OFFICE NAME AND ADDRESS: AFOSR/ NA, Bolling AFB, DC 20332	12. REPORT DATE: December 15, 1982
	13. NUMBER OF PAGES: 65
14. MONITORING AGENCY NAME & ADDRESS(if different from Controlling Office)	15. SECURITY CLASS. (of this report): UNCLASSIFIED
	15a. DECLASSIFICATION DOWNGRADING SCHEDULE

16. DISTRIBUTION STATEMENT (of this Report)

Approved for public release;
distribution unlimited.

17. DISTRIBUTION STATEMENT (of the abstract entered in Block 20, if different from Report)

18. SUPPLEMENTARY NOTES

19. KEY WORDS (Continue on reverse side if necessary and identify by block number)

Three dimensional shock wave/boundary layer interaction
Skewed shock wave
Laminar boundary layer

20. ABSTRACT (Continue on reverse side if necessary and identify by block number)

An experimental study of a 3D skewed shock wave laminar boundary layer interaction has been carried out. The test configuration was a flat/finned plate arrangement with sharp leading edge fins having 4, 6 and 8° incidence relative to the free stream. The flat plate laminar boundary layer had thickness between 1.1 and 2.2 mm depending on test conditions. The unit Reynolds numbers used were 1.2, ~~10^6~~ and 2.4 ~~10^6~~ /m.

Experimental surface data represented as surface flow visualizations and pressure distributions are presented for all test conditions. All tests were carried out at a nominal free stream Mach number of 2.25 and under approximately adiabatic wall conditions. The experimental results indicate that extended separation occurs even for the smallest wedge incidence, i.e., for a pressure ratio of 1.27 and that the extent of upstream influence is much larger in this 3D interaction than in comparable 2D interactions.

Preliminary theoretical investigations show that an integral method is not suited for the study of the present interaction. The new implicit corrected viscosity—

DD FORM 1 JAN 73 1473 EDITION OF 1 NOV 65 IS OBSOLETE

UNCLASSIFIED

method for solving the compressible Navier-Stokes equations can yield convergence speeds of order unity under suitably chosen conditions.

TABLE OF CONTENTS

LIST OF SYMBOLS

p	static pressure	(Nm^{-2})
x-y	Cartesian coordinates in plate plane	(m)
x_F	distance from plate leading edge to fin apex	(m)
Lu	extent of upstream influence	(mm)
LSH	distance from the fin apex along the shock wave	(m)
M	Mach number	
P_0	stagnation pressure	
Re_u	unit Reynolds number	(m^{-1})
α	wedge incidence	
β	shock wave angle	
δ	boundary layer thickness	

Subscripts

i	incipient separation
n	normal

LIST OF FIGURES

1. INTERACTION

The interaction of shock waves with boundary layers has long interested researchers in fluid dynamics, because it is a phenomenon of considerable practical importance in such problems as flows over wings, control surfaces, through engine intakes or across transonic cascades. However, despite the extensive work carried out in the field, there remain many fundamental unanswered questions for the three dimensional case.

In particular, the interaction of a boundary layer with a perpendicular oblique (skewed) shock wave has attracted much interest both because of its geometrical simplicity and of its practical importance. For practical applications, the incoming boundary layer is turbulent and this is why most of the research has been done on this type of interaction (Refs. 1-8).

A series of studies was conducted at Princeton University on this topic with the sponsorship of AFOSR and other agencies (Army Research Office, Naval Air System Command, NASA). They led to a better understanding of the parameters of importance which determine the scale and characteristics of this interactive flow field (Ref. 9). The detailed flow field measurements performed by Oskam (Ref. 6) also serve now as test data for comparison with numerical solutions using full compressible Navier Stokes equation solvers (Ref. 10).

Nevertheless, the fundamental mechanism of the interaction is still unknown and it appears relevant to go back to the study of the more simple laminar interaction case, as was done for the two dimensional interaction. Moreover, the testing of the computer codes solving the Navier-Stokes equations can more suitably be done in the laminar than in the turbulenct case since there is no uncertainty brought out by the turbulence level.

Therefore, a program of studies was established, aiming at determining the basic characteristics of the laminar boundary layer/skewed shock wave interaction in order to discover its key parameters. Surface flow visualizations and surface pressure measurements were made over a wide matrix of flow parameters (Reynolds number, boundary layer thickness, shock strength). The results of the tests are described in detail in section 3. In particular, the variation of upstream and downstream influences as a function of the flow quantities was examined and compared with their two dimensional or turbulent counterparts.

Simultaneously, theoretical investigations were undertaken. Integral methods have proved valuable for the prediction of 2D laminar boundary layer/shock wave interactions (Ref. 11). Some attention was given to the possibility of extending such a method to the computation of a quasi three dimensional plane flow (see section 4). Recently, various numerical techniques were proposed to solve the full compressible Navier Stokes equations (Ref. 12-14) among which is the implicit corrected viscosity technique proposed at the VKI. A preliminary investigation of this method was performed and the results are presented in section 4.

The possibility of performing Laser Doppler Velocimetry measurements is treated in section 5, section 6 presents the conclusions of this report.

2. FACILITY AND INSTRUMENTATION

2.1 Wind tunnel facility

The experiments were carried out in the supersonic wind tunnel S-1 at the von Karman Institute. This is a continuous closed circuit facility of the Ackeret type with a 40 cm × 40 cm test section. The range of stagnation pressure is from 0.1 to 0.3 bar. The Mach number 2.25 nozzle was selected to perform the experiments. This gives unit Reynolds numbers in the ranges 10^6 to 310^6/m. The models were at near adiabatic wall temperature for all tests.

2.2 Test model and instrumentation

2.2.1 General description

The model consisted of a sharp leading edge flat plate, together with a series of wedges with incidences α = 4,6,8,10 and 15° with respect to the free stream. It is shown in figure 1. The wedges were 15 cm high in order to avoid any interference from edge effects and 18 cm long. They could be fixed on the plate at three different longitudinal stations, i.e., with their apex at x_F = 6,9 or 12 cm from the flat plate leading edge. This provided boundary layer thicknesses ranging from 1.1 to 2.2 mm with unit Reynolds numbers of 1.2 and 2.4 10^6/m. Therefore, the Reynolds number based on δ was varied between 1800 and 3600. The flat plate spanned the tunnel and was 60 cm long.

The flat plate was instrumented with four rows of pressure taps parallel to the free stream direction (i.e., wind tunnel axis) at lateral positions of y = 1,5,9 and 13 cm from the wedge apex location. These positions were selected after examining surface flow visualization patterns (see chapter 3). The diameter of the pressure taps was 1 mm. The inside diameter of the tubing was 0.75 mm.

The pressure tappings were studied using 12 port model N0601/1P-12T scanivalves equipped with Validyne DP15 transducers. The scanivalves were automatically controlled by a microprocessor PET Commodore CBM 3032. The output of the transducers was also treated by this microprocessor system. With this on-line system shown in figure 2, tabulated pressure distributions could be obtained immediately following a test.

2.2.2 Surface flow visualizations

Surface flow visualizations were performe ing an oil-graphite mixture. This was adapted from a kero e-graphite technique used at Princeton (Ref. 15). To do this, shorter flat plate was built in order to fit into the S-1 t l injection mechanism. Its fore part was coated with the raphite mixture prior to the test and it was then injected into the tunnel. The oil flowed, leaving on the surface graphite particles which produced the visualization. The pattern was recorded by lifting it off using transparent tape and then sticking it on white paper. On figure 3 is shown a photograph of the model after a test.

2.2.3 Shock wave position

As mentioned by Dolling et al. (Ref. 9), it is important to have an accurate measure of the shock angle β with respect to the free stream. This is not very different from the theoretical oblique shock wave but slight errors in the value of β may lead to significant inaccuracies in shock wave position at large lateral distances. The value of β is approximately constant spanwise expect near the wedge apex, which ensures that the shock wave is effectively plane spanwise.

The position of the shock wave was measured using a pitot probe (Ref. 16) and locating the pressure rise through the shock wave. A lateral traverse mechanism was mounted on a sting

which could be moved vertically and longitudinally. Lateral displacement was measured electrically whereas longitudinal and axial displacements were measured with mechanical counters.

3. EXPERIMENTAL PROGRAM

3.1 Surface flow visualizations

Surface flow visualizations were obtained for the following experimental conditions : α = 4°, 6° and 8°; x_F = 6,9 and 12 cm; Re_u = 1.2 10^6/m and 2.4 10^6/m. Typical examples are shown in figures 4 and 5. Only the flow upstream of the separation line was visualized as it proved to give bad results to introduce oil near the fin to visualize the flow behind the separation line. Additionally, visualizations were performed at α = 10° and 15° in order to check the laminarity of the interaction under critical conditions. This will be treated later in section 3.5.

Several observations can be made when examining these visualizations. The first and probably most striking one is that a separation line can be observed even for the weakest wedge incidence (4°), i.e., for an inviscid pressure ratio of only 1.27. This, according to the terminology of Peake et al. (Ref. 17) is a global separation line since its emanates from a saddle point*. This global character is further proved by the absence of oil behind the separation line. The extent of the separated region is considerable. When this is compared with the two dimensional wedge angle needed to induce incipient separation as computed using the formula by Riethmuller et al. (see Ref. 18).

$$\alpha_i = \frac{37\sqrt{M_\infty}}{Re_{x_F}\ 0.22}$$

---

* There must exist a saddle point because locally, the wedge being blunt, there is a nodal point of attachment on it and because

one realizes that, for the experimental conditions used, this varies between 3.5 to 4.7° depending on x_F and Re_u. Therefore, for a two dimensional interaction yielding the same inviscid pressure ratio, the flow would be attached (for small Re_{x_F}) or would exhibit a small amount of separation (for large Re_{x_F}) whereas in this case, an extended separation is observed in all cases.

When comparing the shape of the separation lines at different wedge incidences, one observes that the Reynolds number effect, if any, is small. The effect of shock strength on the other hand, is measurable but most of it is due to the outward displacement of the shock wave when the wedge angle is increased. This is in contrast with two dimensional interactions when the separation length is strorgly depending on shock strength (Refs. 19,20). For reasons related to model construction, the wedges were asymmetrical, i.e., the incidence and the angle of the other surface with respect to the free stream were not the same. This has no effect on the inviscid flow field since the two flows are independent of one another. On the contrary, it proved to have an effect on the viscous flow. Indeed, when one observes the flow visualization for a small wedge incidence, the separation line is attached to the wedge apex (Fig. 4). For larger incidences, the separation line is ahead of the wedge and its most forward position does not lie on a longitudinal axis passing through the wedge apex, due to the asymmetry of the wedge. This seems similar to the phenomenon of shock detachment in inviscid supersonic flows and would be worth theoretical investigation. Such a phenomenon can also be perceived in figure 6 taken from Korkegi (Ref. 2).

In three dimensional flow fields, there are some particular quasi two dimensional ones which are labelled conically or cylindrically symmetric. For example, the three dimensional hypersonic corner flow (Ref. 21) is of the conical type (Fig. 7). In the present case, the separation line is linear near the wedge apex (except when detached from it), then

becomes curved. The question can be posed whether the interaction reaches cylindrical symmetry far from the wedge apex, i.e., whether all variables become constant along lines parallel to the shock wave. This question cannot be answered by the flow visualization since one cannot observe any region where the separation line runs parallel to the inviscid shock wave but this could be due to an insufficient size of the model. A theoretical discussion of the issue will be presented in chapter 4.

By varying the wedge height, it was verified that for the largest height, the flow could be supposed of the semi-infinite type in the region of interest for the measurements.

3.2 Experimental determination of the shock wave position

The first fact that appeared during these measurements was the importance of the height of the fin, expecially at large lateral distances. The existence of possible edge effects can be estimated by a simple theory which is explained in the following. Consider the experimental configuration shown in figure 8. The Mach cone originating from the tip of the wedge (labelled A in the figure) intersects the shock wave plane along a straight line AB. Since the flow is essentially inviscid in that part of the flow field, it can be stated that the shock wave is plane below line AB. Now, the condition for studying a semi-infinite interaction is that the shock wave is effectively plane when submitted to interaction with the boundary layer. Since line AB is going down as distance is increased away from the wedge tip, there will be a limiting distance at which the shock wave is no longer plane. From reference 22 it is known that the height of the interaction region is approximately δ, thickness of the incoming boundary layer. Since this is only a few millimeters, it will be neglected with respect to the wedge height and the limit distance will be calculated as the one which corresponds to the intersection of line AB with

the flat plate. This can easily be calculated using the geometrical relations layed out in figure 8. Once the angle γ of inclination of line AB is known (see Fig. 8), the position of its intersection with the flat plate is easily computed, in particular its lateral distance from the wedge root R. For h = 15 cm, M_1 = 2.21, and α = 4,6 and 8°, the values of this lateral distance are 31.8 cm, 27 cm and 24 cm. These are well beyond the largest distance considered in the pressure measurements (y = 13 cm). Therefore, the interaction may be considered of the semi-infinite type for all test conditions.

A first series of experiments was conducted by exploring the flow with a pitot probe at different heights over the flat plate, with a wedge 5 cm high. The location of the sharp pressure rise associated with the shock wave never reached an asymtotic value as the height over the flat plate was increased, proving that the interaction was not of the semi-infinite type, as could be predicted from the previous analysis. Subsequently, the experiment was repeated with a wedge 15 cm high. Then an asymptotic value was noticed for all wedge incidences and all Reynolds numbers. In order to verify that these values were indeed associated with the inviscid shock wave, the experiment was redone, in which just the wedge was placed in the tunnel, without the flat plate thus avoiding any interference from the shock/boundary layer interaction. Values for the shock locations in agreement with the previous "asymptotic" values were recorded. Nevertheless, some problems remained. First, the shock wave angle as determined by the measured position, constant in the spanwise direction except near the wedge apex, was greater than the theoretical value by as much as 2° for the lowest Reynolds number whereas the difference was never greater than 0.3° in Dolling's experiments at Mach 3 (Ref. 9), conducted, however, at much higher Reynolds number. Second, there was a marked effect of unit Reynolds number, the measured shock wave angle being reduced by 1° when changing Re_u from 1.2 10^6/m to 2.1 10^6/m. Third, the pressure distributions recorded with the pitot probe moving axially exhibited some strange behaviour.

Instead of measuring a steplike distribution, the pressure decreased immediately after the shock wave when moving downstream. This could not be attributed to edge effects. This sheds doubts about the sense of the measure and raises the issue of the existence of a systematic error due to the measurement technique.

The results being inconclusive, they will not be used. A comparison with optical visualization could help clarify this issue.

3.3 Surface pressure measurements

Surface pressure measurements were obtained for the same experimental conditions, i.e., $\alpha = 4°,6°$ and $8°$; $x_F = 6,9$ and 12 cm; $Re_u = 1.2\ 10^6$ and $2.4\ 10^6$/m. Pressure distributions were recorded at lateral distances y = 1,5,9 and 13 cm. Typical examples when the pressure is non dimensionalized by stagnation pressure ahead of the shock, P_0, are represented in figures 9 to 11. Each figure shows the pressure distribution at differens y's for given α, x_F and Re_u. Pressure distributions are shown as a function of the distance x from the flat plate leading edge. Also indicated on the figures are the locations of the theoretical shock wave and of the separation line as observed from the visualizations together with the inviscid pressure values upstream and downstream of the shock wave. Clearly, from the measured distributions, it can be stated that the pressure tappings did not cover the entire interaction region. In order to obtain complete information about the flow, new tappings should be designed and the tests should be redone. This is the object of the research proposal submitted as a continuation of grant AFOSR 82-0051.

By examining the pressure distribution, some general observations can be made. For all shock strengths and all lateral distances, the pressure distribution can be divided in two parts. Upstream of the inviscid shock wave, there is a pressure rise constant in magnitude whenever the lateral

distance or Reynolds number are, and varying little with shock strength. This is followed, downstream of the inviscid shock by a rather sharp pressure rise. The curve overshoots the inviscid pressure value as calculated from oblique shock theory, then relaxes to the inviscid value. The pressure rise in the second part of the distribution depends thus strongly on the shock strength value since the overall pressure rise must be equal to the inviscid pressure rise. The overshoot in the pressure distribution is probably due to an attachment phenomenon. A similar division of the pressure distributions in two parts was also noticed in the turbulent case (Ref. 6) when separation is present.

For the skewed shock wave turbulent boundary layer interaction, it is shown in figure 12 (taken from Ref. 6) that for incidences greater than 9°, the pressure at the position of the inviscid shock wave is little affected by a change in shock strength whereas the downstream pressure rise changes significantly. Also, when comparing pressure distributions in isobar form (also from Ref. 6) taken with two different boundary layer thicknesses (Figs. 13,14), it can also be noticed that the pressure at the location of the shock wave does not vary with lateral distance and is approximately the same in both cases.

In pressure distributions encountered in the blunt fin induced shock wave turbulent boundary layer interaction, Dolling et al. (Ref. 23) also noticed the division of the pressure distribution in two parts, the first of which consisted in a pressure rise whose magnitude varied little as lateral distance from the centerline was increased or as the fin leading edge geometry was altered. Such a behaviour thus seems to be a characteristic feature of three dimensional interactions.

In the present work, the pressure level at the location of the shock was approximately 1.12 p_2. This is of the same order of magnitude as the pressure at separation for a two dimensional interaction. For M = 2 and the various Reynolds numbers

used, the latter varies between 1.12 and 1.17 p_1. It is important to note, however, that in the two dimensional case, the pressure level at separation varies strongly with Reynolds number whereas the pressure rise in the three dimensional separation line is much lower than the latter value (see Figs. 9-11).

Finally, all pressure distributions exhibit a kink near the inviscid shock wave location. This kink tends to become a trough as lateral distance Y is increased. A similar trend in also observed when Reynolds number increases. Such a kink is generally associated with the existence of separation in two dimensional interactions (Ref. 20).

A useful piece of information which can be systematically extracted from the pressure distribution is the extent of upstream influence. In order to render more precise the determination of upstream influence, it has been defined, as indicated in figure 15, the straight line appearing in the drawing being the tangent to the pressure distribution at the inflexion point. The values of upstream influence in functions of Re, α, x_F are presented in Table I. From the examination of the dimensional quantities, several observations can be made.

First, there is hardly any effect of shock strength on the amount of upstream influence. This is in sharp contrast with two dimensional interactions where the shock strength is the leading parameter in the determination of upstream influence. A discussion of this phenomenon will be presented in chapter 3.6. On the contrary, the downstream influence depends on shock strength : it decreases as shock strength increases. This is also in sharp contrast with two dimensional interactions, where downstream influence varies in the same sense as upstream influence when shock strength is increased, i.e., they both increase. A possible explanation is offered for the decrease in downstream influence as shock strength is increased in the three dimensional case : when shock strength is increased, the longitudinal distance between the shock wave and the shock generator decreases.

There is therefore less "room" for downstream influence.

Second, for α and x_F given, there is no consistent trend of the data when changing unit Reynolds numbers. On the contrary, for a given unit Reynolds number, there is a consistent increase in upstream influence as x_F is increased.

The most useful observation of the data being in non dimensional form, a non dimensional plot of Lu/δ as a function of LSH/δ was made (for a definition of LSH, see Fig. 1) (Fig. 15). The value of δ used in the non dimensionalization process was the value at the fin apex, as given by the theory of Chapman and Rubesin (Ref. 24). This particular way of presenting the data was chosen because it proved to be the suitable choice of parameters in the turbulent case (Ref. 15). By dimensional analysis, it can be shown that with these parameters chosen, the general formula for Lu/δ reads :

$Lu/\delta = f(LSH/\delta, Re\delta, \alpha)$ for a fixed Mach number.

In the laminar case too, the data fit onto a single band of points. The scatter of data is due to uncertainties in the experimental values, which will be discussed in chapter 3.4. Because of this scatter, it is impossible to determine whether there is an influence of shock strength and Reynolds number based on the curve $Lu/\delta = f(LSH/\delta)$. As an improvement of the quality of measurements is expected for the new series of experiments, it is hoped that the identification of the influence of any single parameter will be possible. A theoretical analysis similar to that of Settles et al. (Ref. 26) will be presented in chapter 3.6 in order to predict the effect of $Re\delta$.

From figure 15, it can be seen that nowhere is cylindrical symmetry achieved. This does not necessarily mean that the semi-infinite interaction can never reach cylindrical symmetry. It just means that in the experimental simulation, edge effects are encountered before the hypothetical appearance

of cylindrical symmetry. Yet, the quantity LSH/δ is already large when edge effects are susceptible to appear and it is probable that this type of interaction never reaches cylindrical symmetry. Furthermore, there is a strong theoretical argument in this sense which will be discussed in chapter 3.6.

Finally, a typical pressure distribution is compared to a typical two dimensional pressure distribution taken by Burgio (Ref. 27) at M = 2.2 , α = 7.5°, P_0 = 79 mm Hg (which under normal conditions of temperature gives Re_u = 1.16 10^6/m, X_F = 6 cm). On figure 16 appears the pressure distribution by Burgio and the pressure distributions in the three dimensional interaction for α = 8°, Re_u = 1.31 10^6/m, x_F = 6 m at the various lateral positions. Major differences can be observed. First, the shape of the pressure distribution is radically different. There are two non exclusive possible reasons for this difference. The interaction, when viewed in a plane perpendicular to the shock wave is that of a boundary layer with a "normal" shock wave, not an oblique one. Also, the introduction of three dimensionality does not simply reduce to the existence of a cross flow but modifies completely the mechanics of the interaction. Second, as lateral distance is increased, the upstream and downstream influences of the interaction become much larger than that of the two dimensional interaction yielding the same pressure ratio. This favours the point of view that the mechanism of the interaction is radically different from that of the two dimensional interaction : if it was similar, one would expect that, far from the wedge apex, the interaction would become quasi two dimensional with cross flow. As is shown by a calculation using Lees-Reeves integral method (Ref. 28) in such a case, the effect of cross flow is small. Therefore, the amount of upstream influence would reach values of the same order as those encountered in two dimensional interactions far from the wedge apex. This is in contradiction with the experimental observation.

In conclusion, the major observations made from the pressure distributions are the following : for all test cases, there is a considerable extent of the region disturbed by the interaction. This extent is so large that it was not entirely covered by the present tappings. It depends very weakly on shock strength and not measurably on Reynolds number. The pressure distribution can be divided into two parts (ahead and downstream of the inviscid shock wave) which behave differently.

3.4 Uncertainties in the measurements

3.4.1 Flow visualizations

The flow visualization technique involves some difficulties due to the nature of the wind tunnel. At Princeton (Ref. 15) a kerosene graphite technique is used with much success. Unfortunately, it was not possible to use this technique in the S-1 facility for the following reason. Since the VKI tunnel operates at reduced pressure, it needs a long pumping time before starting the flow; during this time the kerosene evaporated. Therefore, the kerosene had to be replaced by a fluid which would not evaporate during the pumping time. Oil was selected because, as it flowed on the model, it left the graphite particles which produced the visualization. Nevertheless, the quality was much poorer than when using the kerosene graphite technique because in the latter case the surface streamlines are much more accurately drawn.

Furthermore, due to the inertia of the oil, it flowed past the separation line when injecting the model. At the steady state, as the test was still being performed, the separation line could clearly be observed but after shutdown, there was some uncertainty due to the initial flow of the oil past the separation line. Therefore, the method is only qualitative and only major trends can be observed.

3.4.2 Surface pressure measurements

The pressure measurements have been hampered by several difficulties. First, due to the availability of the data acquisition system, the number of transducers was increased in order to take the most advantage of the microprocessor abilities. This induced severe leak problems in the tubings, which were not completely solved. Second, there appeared an important zero shift of the transducers during operation, so that it was necessary to make a zero correction of the data. The errors involved in the process as well as those due to the existence of small leaks are such that the pressure distributions obtained at present are only qualitative. They also introduce an uncertainty in the Mach number determination.

3.5 Laminarity of the interaction

The laminarity of the interaction is an important issue because it is essential that it be ensured to allow comparison with other experimental data or with a theoretical prediction. However, this problem is much more complicated than in a two dimensional experiment. In a two dimensional experiment, the occurrence of transition after the reattachment point ensured the laminar state of the interaction because the transition did not exert any upstream influence is such a case. This could not be checked experimentally by a direct method but Ginoux (Ref. 29) proposed an equivalent criterion based on the variation of upstream influence with Reynolds number. For the three dimensional configuration under study, however, transition can occur not only longitudinally but also laterally in the interaction region. The problem is then to evaluate the extent of influence of transition on the features of the interaction. This problem was addressed by Korkegi (Ref. 28) in the case of a supersonic corner. It was noticed that a characteristic bend (Fig. 7) occurs in the separation line at the location where transition takes place. This was never encountered in

the present test series, not even for α = 10 or 15°. As a matter of fact, the experimental conditions were chosen such that an equivalent two dimensional interaction would be in a fully laminar state. That observation thus strongly supports the laminar character of the tests performed, since there is no apparent effect on the surface flow visualization. In addition, the very large extent of separated flow supports the laminar nature of the test and the weak upstream influence of transition. Nevertheless, as long as there is no theoretical prediction of the upstream extent of influence of transition, it is difficult to assess exactly which part of the flow can actually be considered of the laminar type.

3.6 Discussion of the results

In this section, the question of the effect of Reynolds number and the question of cylindrical symmetry will be discussed as announced in chapter 3.3. In addition, a tentative explanation of the differences between two dimensional and three dimensional interactions will be proposed.

The Reynolds number effect on three dimensional shock/turbulent boundary layer interactions was studied in two papers by Settles et al. (Ref. 16) and Dolling (Ref. 9), using dimensional analysis. Starting from the two dimensional formula for upstream influence as a function of various parameters

$$Lu/\delta = 0.9e^{0.23\alpha} Re_\delta^{-1/3} \quad \text{for } M = 3 \qquad (1)$$

they looked for a three dimensional generalization. The general formula for upstream influence in the skewed shock wave boundary layer interaction being

$$Lu/\delta = f(LSH/\delta, Re_\delta, \alpha, M) \qquad (2)$$

they assumed that the dependence on Reynolds number in the three dimensional case would exhibit the same form as in the two

dimensional case, namely they restricted the most general expression to a single one

$$\frac{Lu}{\delta} / Re\delta^{a} = f\left[\frac{LSH}{\delta} / Re\delta^{b}, \alpha, M\right] \qquad (3)$$

When compared to the experimental data this expression was able to correlate the experimental data and a and b had the common value of 1/3 which was already used for two dimensional scaling Moreover, it was found that the upstream influence was not a function of the two independent variables M and α but only of a combination of the two, namely the normal Mach number $Mn = M\sin\beta$ (for M and α fixed, β is known). If an analogous development is performed in the laminar case, the two dimensional relation being :

$$\frac{Lu}{\delta Re\delta^{3/2}} = f(M,\alpha) \qquad (4)$$

the three dimensional relation will read :

$$\frac{Lu}{\delta Re\delta^{3/2}} = f\left[\frac{LSH}{\delta Re\delta^{3/2}}, Mn\right] \qquad (5)$$

This relation remains to be checked experimentally.

The cylindrical symmetry of the interaction is also a problem which has been posed a long time ago by McCabe (Ref. 1) in the turbulent case. Examining results in a similar geometry, Nebbeling (Ref. 30) concluded that the interaction could be divided in several regions (Fig. 18). From that figure, it can be stated that, even if the separation line runs parallel to the inviscid shock wave, the flow may never be purely of the cylindrically symmetric type since the distance between the shock wave and the wedge keeps increasing as one progresses laterally (see "conical region" behind "two dimensional region" in Fig. 18).

As discussed earlier, important differences appear between the behaviour of two dimensional and three dimensional interactions. In particular, the appearance of separation and the amount of upstream influence are two important features different in both types of interactions. This is due to the fundamental difference in nature between two dimensional and three dimensional separation. Recently, the issue of three dimensional separation, which has been controversial since the pioneering papers of Maskell (Ref. 31) and Eichelbrenner et al. (Refs. 32,33), has been clarified by a significant contribution from Peake and Tobak (Refs. 17,22,34). From continuity arguments and topological considerations, the nature of separation in flows over simple configurations was established and flow models presented. A major difference which exists between two dimensional and three dimensional separated flows clearly appears on figure 19 where are shown possible flow patterns in the plane of symmetry ahead of a three dimensional obstacle and two dimensional flow pattern ahead of a step. The major difference can be stated as follows : in two dimensional flow, it is impossible to draw a path from the separated region to the upstream infinity without crossing the dividing line whereas in three dimensional flow, the "separated region" is continuously fed by fluid coming from upstream. A most spectacular example of this is the flow over a delta wing. To state the same thing in another way : in two dimensional flow, a separated region is really separated from upstream infinity by the dividing line, whereas in three dimensional flow, this is untrue : as pointed out by Korkegi (Ref. 4), there is a certain amount of mass transfer toward the separated region. The importance of this mass transfer is of greatest importance in the nose region of a blunt fin induced shock wave boundary layer interaction as mentioned in reference 35. Therefore, the word separation does not carry the same sense in two dimensional and three dimensional cases. A consequence of the mass transfer is that, if the reattaching streamline comes from outside the incoming boundary or from high energy layer in the boundary layer, the boundary layer which develops behind the separation line is a

"new" boundary layer, independent of the incoming boundary layer characteristics. This is the reason for the very high heat transfer rates encountered in three dimensional hypersonic separated flows.

Yet, there are examples of three dimensional flows in which separation exhibits features very close to that of two dimensional separated flows, an example of which is shown in figure 20, together with the equivalent two dimensional configuration. In this case, the mass transfer towards the separated region is so small that the flow may be considered of the two dimensional type. This is of course the basis for carrying out two dimensional experiments.

The previous discussion paves the way for establishing a criterion for the classification of the various three dimensional shock/boundary layer interactions. It is obvious that the mechanism of three dimensional separated flows is radically different in the cases of large or very small mass adjunction in the separated region. Therefore, a qualitative estimation of the mass adjunction would provide a suitable criterion for distinguishing the various three dimensional separated flows.

4. THEORETICAL INVESTIGATIONS

As mentioned in the introduction, a theoretical investigation was performed. Two approaches were studied in more detail : the newly proposed corrected viscosity method for solving the full Navier Stokes equations and a possible extension of the Lees-Reeves integral method.

For solving these kinds of flow problems where there is a strong coupling between viscous and inviscid flow there are essentially two approaches. The first one consists in solving the full Navier-Stokes equations while the second consists of performing a coupled computation of an inviscid external flow field with a boundary layer.

The first type of method uses finite difference or finite element techniques for discretizing the Navier-Stokes equations. This renders the methods very general, so that after a major initial effort, many flow configurations could be studied. To this category belong the methods of McCormack (Ref. 12), Beam and Warming (Ref. 13), and the implicit corrected viscosity method recently proposed by a VKI faculty member, Prof. Essers (Ref. 14) (the latter method is studied in further detail in chapter 4.1). Their main disadvantage is that they require considerable storage space and long computing times.

Among methods using a coupling approach (which are discussed in detail by Le Balleur, Ref. 36), the integral method in general and the integral method of Lees-Reeves (Ref. 11) in particular offer the advantage of a reduced storage requirement or computing time, with the disadvantage of a small flexibility. Since the VKI has considerable experience with these methods, the possibility of adapting the work of Leblanc (Ref. 28) to the present flow configuration was studied (Chapt. 4.2).

4.1 Implicit corrected viscosity method for solving the compressible Navier-Stokes equations

Presently, the two most effective methods for solving the full compressible Navier-Stokes equations are McCormack's (Ref. 12) and Beam and Warming's (Ref. 13). The main advantage of McCormack's method is that it needs the solution of block bidiagonal systems whereas block tridiagonal systems should be solved in Beam and Warming's method. On the other hand, Beam and Warming's method has the big advantage that the precision of any steady state solution is independent of the time step used in the marching process.

Recently, new methods based on the principle of implicit corrected viscosity were proposed (Ref. 14). Their principle is as follows - suppose that the steady state equations to be solved are the following :

$$D_i(\vec{S}) = 0 \qquad i = 1, \ldots M \qquad (1)$$

D_i being space differential equations applied to the unknown vector $\vec{S}$. They correspond to the steady part of compressible Navier-Stokes equations or a combination thereof. The unsteady equations solved in all classical time dependent techniques can be written as :

$$\frac{\partial Si}{\partial t} = D_i(\vec{S}) + \lambda V_i(\vec{S}) \qquad (2)$$

where λ is a small positive constant and the V_i's are space elliptic aritificial viscosity operators possibly used to avoid non linear instabilities, when hyperbolic equations are to be solved. As the artificial viscosity introduces errors to the steady solution, λ should obviously be kept small. This limits the speed of convergence of the method. To significantly improve the rate of convergence, Couston, McDonald and Smolderen (Ref. 37) proposed a so-called corrected viscosity

approach. In that technique, the following equations are solved :

$$\frac{\partial Si}{\partial t} = D_i(\vec{S}) + \lambda\left[V_i(\vec{S})-V_i(\vec{S}^*)\right] \qquad (3)$$

$\vec{S}^*$ being the vector $\vec{S}$ computed at some previous iteration. At steady state, $\vec{S} = \vec{S}^*$ and therefore, the accuracy of the solution does not depend on the quantity λ. On the other hand, the introduction of the correction term does not alter the damping qualities of equation (2). The method is therefore expected to yield faster convergence speeds than existing methods. This has proved to be the case for explicit corrected viscosity techniques which have been successfully used for various transonic problems including aerofoil and cascade flows.

What is proposed here is to use implicit corrected viscosity schemes. Essers has proved (Ref. 14) that the use of a one step fully implicit scheme is not interesting. To overcome this difficulty, it is suggested to perform a splitting of equations (3). In that technique, a series of similar cycles are computed successively at various time levels. Each cycle consists of an explicit physical part followed by an implicit corrected viscosity step. This has the further advantege that, if complicated turbulence models have to be introduced in the physical equations, they would be introduced explicitly and would not require the calculation of complicated jacobians as required by the methods of Beam and Warming or McCormack. The explicit schemes could be composed of several steps but should be dissipative for all wavelengths. The corrected viscosity steps consist of correcting the explicitly predicted value $\hat{S}^{\ell+1}$ by solving the following equation :

$$\vec{S}^{\ell+1} = \hat{S}^{\ell+1} + \lambda\Delta t\left[V_i\left(\vec{S}^{\ell+1}\right) - V_i(\vec{S}^*)\right] \qquad (4)$$

This could be done by overrelaxation methods or more efficiently by multigrid techniques.

This method was studied and tested over a simple one dimensional test case (Ref. 38). It proved to be efficient. The extension to two dimensional cases was studied theoretically using a Von Neumann analysis. The results are presented in detail in reference 34. Let us here briefly state the major findings. Suppose that the equation to be solved reads :

$$\frac{\partial u}{\partial t} + a \frac{\partial u}{\partial x} = \frac{\partial^2 u}{\partial x} \qquad (5)$$

it is a one dimensional equation involving both conduction $\left(a \frac{\partial u}{\partial x}\right)$ and diffusion $\left(\varepsilon \frac{\partial^2 u}{\partial x^2}\right)$. It thus figures the the features of fluid flow.

Among explicit schemes which can be used to compute the physical step, the Lax Wendroff 2-step scheme exhibits a major advantage. If it is used to solve equation (5) the scheme will read :

LW First step :

$$u_m^{\ell+1} = \frac{1}{2}\left(u_{m+1}^{\ell} + u_{m-1}^{\ell}\right) - a\Delta t \frac{\partial u^{\ell}}{\partial x m} + \varepsilon \Delta t \frac{\partial^2 u_{\ell}}{\partial x^2 m}$$

LW Second step :

$$\tilde{u}_m^{\ell+2} = u_m^{\ell} - 2a\Delta t \frac{\partial u^{\ell+1}}{\partial x m} + 2\varepsilon\Delta t \frac{\partial^2 u^{\ell+1}}{\partial x^2 m}$$

Corrected viscosity :

$$u_m^{\ell+2} = \tilde{u}_m^{\ell+2} + 2\mu\Delta t \left[\frac{\partial^2 u^{\ell+2}}{\partial x^2 m} - \frac{\partial^2 u_{\ell}}{\partial x^2 m}\right]$$

It has been proved (Ref. 33) that the faster convergence speed is obtained for $u^{\ell+2} = u^{\ell}$, which means that the viscous term should be corrected by the previous time step value.

In such a case, the latter two steps can be combined and written in Δ form.

$$\Delta u^{\ell} = u^{\ell+2} - u^{\ell}$$

$$\Delta u_m^{\ell} = - 2a\Delta t \frac{\partial u^{\ell+1}}{\partial xm} + 2\varepsilon\Delta t \frac{\partial^2 u^{\ell+1}}{\partial x^2 m} + 2\mu\Delta t \frac{\partial^2 \Delta u^{\ell}}{\partial x^2 m}$$

This proves one advantage of the scheme (shared by that of Beam & Warming) : the accuracy of the converged solution (time level $\ell+1$) does not depend on the time step used.

When a stability analysis of the scheme is performed (Ref. 39) it is shown that with suitable discretization of the spatial derivatives, the stability and convergence speed of the scheme depends on two parameters

$$\theta = \frac{a^2 \Delta t}{\mu} \qquad \lambda = \frac{\omega \mu}{a}$$

where ω is the pulsation of the mode under study. For each λ there is an optimum value of θ ($\neq 1$) which maximizes the convergence speed. On the contrary, it appears that there is no limit on λ. For increasing λ, one should get increasing convergence speed. This will probably be limited by boundary conditions or non linear instabilities.

Yet, a convergence speed of order unity may be obtained using such a method. The extension to two dimensional problems can easily be done. The qualities of the method are conserved. This very encouraging result ranks the method among the most promising ones.

4.2 Extension of Lees-Reeves integral method

Following the works of Leblanc (Ref. 28) who introduced the effect of cross flow in an axisymmetric interaction between a shock wave and a laminar boundary layer, it was envisaged to extend this method to compute a cylindrically symmetric normal shock/laminar boundary layer interaction with cross flow which would represent the cylindrically symmetric part of a skewed shock/laminar boundary layer interaction.

However, there is a major problem because, the inviscid flow behind the shock being subsonic (in the normal direction), the coupling used by Lees and Reeves (Prandtl Meyer relation) could not be used. A subsonic coupling would by no means be impossible but would be rather involved. Furthermore, the experimental results show no region of cylindrical symmetry for this interaction.

On the other hand, the method appears well suited for the computation of interactions at swept compression corners which is known to exhibit regions of cylindrical symmetry in the turbulence case (Ref. 26). This configuration seems analogous to that studied by Leblanc (Ref. 28) but important differences exist: in this case, the total enthalpy is constant throughtout the boundary layer (for Pr = 1). Also, if sweep is to be introduced for a fixed Mach number, the normal Mach number will vary, which is not the case in the work of Leblanc. This is the reason why the analysis of the method was persued.

A preliminary study was carried out whose results are presented in reference 40. A summary of the analysis is given in Appendix I. This shows that the effect of sweep is analogous to the effect of heating. It is therefore expected that it will have a similar effect as, for instance, increasing the upstream influence.

A computation of the weak interaction region which develops at the leading edge of a plate in supersonic flow was carried out in order to verify this prediction. The results (Fig. 21) show that it is verified. This partly explains the unfavourable effect of sweep on the extent of disturbed regions in shock/boundary layer interaction problems.

5. POSSIBILITY OF PERFORMING LDV MEASUREMENTS IN THE SKEWED SHOCK WAVE/LAMINAR BOUNDARY LAYER INTERACTION

As announced in the original proposal, the possibility of performing LDV measurements in this interaction was evaluated. It appeared that the measurements would present considerable difficulty which would prevent obtaining results in the near future. Yet, a progressive program aiming at performing velocity measurements in this interaction can be constructed. This is the object of a new research proposal to AFOSR.

6. CONCLUSIONS

An experimental investigation of a three dimensional skewed shock wave/laminar boundary layer interaction has been performed. Surface flow visualizations and surface pressure measurements have been carried out over a variety of test conditions. This provided a parametric study of the interaction. Simultaneously, two theoretical approaches were evaluated : an extension of Lees-Reeves-Klineberg integral method and new implicit corrected viscosity methods. The conclusions are :

- The upstream influence is much larger in this three dimensional interaction than in a two dimensional interaction having the same overall pressure rise. So is the downstream influence. This had the consequence that the pressure tappings did not cover the entire interaction region.

- Extended separation occurs even for the smallest wedge incidence, it is for a pressure ratio of 1.27.

- A criterion is proposed to characterize three dimensional interactions and to distinguish between quasi two dimensional interactions and fully three dimensional interactions, the mechanisms of each type being different.

- The integral method of Lees-Reeves-Klineberg is not suited for the analysis of the skewed shock wave/laminar boundary layer interaction. On the contrary, it is well suited for the analysis of the flow at swept compression corners. It indicates that sweep tends to increase upstream influence.

- The newly proposed implicit corrected viscosity method was studied. The analysis shows that by suitably choosing its parameters, convergence speeds or order unity can be achieved.

REFERENCES

1. McCABE, A.: The three dimensional interaction of a shock wave with a turbulent boundary layer.
Aeronautical Quart., Vol. 17, Part 3, August 1966, pp 231-252.

2. KORKEGI, R.H.: Effect of transition on three dimensional shock wave boundary layer interaction.
AIAA J., Vol. 10, No. 3, March 1972, pp 361-363.

3. NEUMANN, R.D. & TOKEN, K.H.: Prediction of surface phenomena induced by three dimensional interactions in planar turbulent boundary layers.
IAF XXV Congress, Paper 74-058, October 1974.

4. KORKEGI, R.H.: On the structure of three-dimensional shock induced separated flow regions.
AIAA J., Vol. 14, No. 5, May 1976, pp 597-600.

5. COUSTEIX, J. & HOUDEVILLE, R.: Epaississement et séparation d'une couche limite turbulente soumise en interaction avec un choc oblique.
Recherche Aérospatiale, 1976-1, jan-fév. 1976, pp 1-11.

6. OSKEM, B.: Three dimensional flow fields generated by the interaction of a swept shock wave with a turbulent boundary layer.
Princeton University, Gas Dynamics Lab., Report 1313, December 1976.

7. PEAKE, D.J.: Three-dimensional swept shock/turbulent boundary layers separations with control by air injection.
Ph. Thesis, Carleton U., Ottowa 1975, also NRC Aero Rept LR 592, 1971.

8. KUBOTA, H. & STOLLERY, J.L.: An experimental study of the interaction between a glancing shock wave and a turbulent boundary layer.
J. Fluid Mechanics, Vol. 116, March 1982, pp 431-458.

9. DOLLING, D.S. & BOGDONOFF, S.M.: Upstream influence scaling of sharp fin-induced shock wave turbulent boundary layer interaction.
AIAA 14th Aerospace Sciences Meeting, June 12-15, 1981, AIAA Paper 81-0336, 1981.

10. HORSTMAN, C.C. & HUNG, C.M.: Computation of three dimensional turbulent separated flows at supersonic speeds.
AIAA Paper 79-0002, 1979.

11. LEES, L. & REEVES, B.L.: Supersonic separated and reattaching laminar flows. I, General theory and applications to adiabatic boundary layer shock wave interaction.
GALCIT, Tech. Report No. 3, 1963.

12. McCORMACK, R.W.: A numerical method for solving the equ - tions of compressible viscous flow.
AIAA Paper 81-0110, January 1981.

13. BEAM, R.M. & WARMING, R.F.: An implicit factored scheme for compressible Navier-Stokes equations.
AIAA J., Vol. 16, No. 4, April 1978, pp 393-402.

14. ESSERS, J.A.: Explicit and implicit corrected viscosity schemes for the computation of steady transonic flows.
Paper presented at the 4th GAMM Conference on Numerical Methods in Fluid Mechanics, Paris, October 7-9, 1981. Also:
VKI Preprint 1982-02.

15. SETTLES, G.S.: An experimental study of compressible turbulent boundary layer separation at high Reynolds number.
Ph.D. Dissertation, Aerospace and Mechanical Sciences Dept., Princeton University, Princeton NJ, Sept. 1975.

16. BANNICK, A.J. & NEBBELING, C.: Determination of the position of a shock wave from pitot tube experiments.
AIAA J., Vol. 9, No. 2, February 1971, pp 345-347.

17. PEAKE, D.J. & TO AK, M.: Three dimensional separation and reattachment. In :
High Angle-of-Attack Aerodynamics,
AGARD LS 121, Paper 1, 15-19 March, 1982.

18. RIETHMULLER, M.L. & GINOUX, J.J.: A parametric study of adiabatic laminar boundary layer shock wave interactions by the method of Lees-Reeves-Klineberg.
VKI TN 60, June 1970.

19. NEEDHAM, D.A. & STOLLERY, J.L.: Hypersonic studies of incipient separation and separated flows. In:
Separated Flows,
AGARD CP 4, May 1966, pp 89-120.

20. GINOUX, J.J.: Interaction entre ondes de choc et couches limites. In:
Chocs et Ondes de Choc, Tome II, Mason 1973, pp 1-65.

21. COOPER, J.R. & HANKEY, W.L.: Flowfield measurements in an asymmetric axial corner at M = 12.5.
AIAA J., Vol. 12, No. 10, Oct. 1974, pp 1353-1357.

22. PEAKE, D.J. & TOBAK, M.: Three dimensional interaction and vortical flows with emphasis on high speed. AGARDograph 252, 1980.

23. DOLLING, D.S. & BOGDONOFF, S.M.: Experimental investigation of three dimensional shock wave turbulent boundary layer interaction - an exploratory study of blunt fin induced flows - Princeton University, Gas Dynamics Lab., Report MAE 1468, March

24. CHAPMAN, D.R. & RUBESIN, M.W.: Temperature and velocity profiles in the compressible laminar boundary layer with arbitrary distributions of surface temperature. J. Aeronautical Sciences, Vol. 16, No. 9, September 1949, pp 547-565.

25. DOLLING, D.S. & BOGDONOFF, S.M.: Experimental study of three dimensional shock wave turbulent boundary layer interaction. Scaling of sharp and blunt fin induced flow field. Princeton University, Gas Dynamics Laboratory, Report 1483, July 1980.

26. SETTLES, G.S.; PERKINS, J.J.; BOGDONOFF, S.M.: Upstream influence scaling of two dimensional and three dimensional shock/turbulent boundary layer interaction at compression corners. AIAA 19th Aerospace Sciences Meeting, Jan. 12-15, 1981. AIAA Paper 81-0334.

27. BURGIO, C.: Comparison between shock wave/boundary layer interactions caused either by incident shocks or ramps. VKI PR 70-266, June 1970.

28. LEBLANC, R.: Effet d'un écoulement transversal sur une interaction onde de choc-couche limite en configuration de révolution. Thèse de Doctorat, U. Libre de Bruxelles, Mars 1971.

29. GINOUX, J.J.: Supersonic separated flows over wedges and flows with emphasis on a method of detecting transition. VKI TN 47, August 1968.

30. NEBBELING, C.: Private communication, 1981.

31. MASKELL, E.: Flow separation in three dimznsions.
RAE Aero Report 2565, 1955.

32. EICHELBRENNER, E.A. & OUDART, A.: Observation sur un critère de décollement laminaire dans la couche limite tridimensionnele.
ONERA Recherche Aérospatiale, Vol. 40, 1954, pp 3-5.

33. EICHELBRENNER, E.A. & OUDART, A.: Le décollement laminaire en trois dimensions.
ONERA Recherche Aérospatiale, Vol. 47, 1955, pp 11-14.

34. PEAKE, D.J. & TOBAK, M.: Three dimensiona. flows about simple components at angle of attack. In:
High Angle-of-Attack Aerodynamics,
AGARD LS 121, Paper 2, 15-19 March, 1982.

35. DEGREZ, G.: Exploratory experimental investigation of the unsteady aspects of blunt fin induced shock wave turbulent boundary layer interactions.
MSE Thesis (1516-T), Mechanical and Aerospace Eng. Dept.,
Princeton University, Princeton NJ, June 1981.

36. LE BALLEUR, J.C.: Viscid-inviscid coupling calculations for two and three dimensional flows. In:
Computational Fluid Dynamics,
VKI LS 1982-04, March 29-April 2, 1982.

37. COUSTON, M.; McDONALD, P.W.; SMOLDEREN, J.J.: The damping surface technique for time dependent solutions to fluid dynamic problems.
VKI TN 109, 1971.

38. KILL, N.: Calcul d'écoulement transsoniques autour de profils d'ailes.
Mémoire du fin d'études, Faculté de Sciences Appl.,
U. Liège, 1981.

39. ESSERS, J.A. & DEGREZ, G.: Fast implicit cor ·cted viscosity techniques for the solution of Euler and Navier-Stokes equations.
VKI TN (in preparation)

40. DEGREZ, G. & ANDRES, P.: An integral analysis for the cylindrically symmetric shock wave/laminar boundary layer interaction at swept compression corners-weak interaction region.
VKI TN (in preparation).

APPENDIX I - LEES REEVES INTEGRAL METHOD FOR SHOCK/BOUNDARY LAYER INTERACTION WITH CROSS FLOW

Under the assumption of cylindrical symmetry and adiabatic conditions, the boundary layer equations read :

Continuity :

$$\frac{\partial}{\partial x}(\rho u) + \frac{\partial}{\partial y}(\rho v) = 0$$

x-momentum :

$$\rho u \frac{\partial u}{\partial x} + \rho v \frac{\partial u}{\partial y} = - \frac{\partial p}{\partial x} + \frac{\partial}{\partial y}\left(\mu \frac{\partial u}{\partial y}\right)$$

z-momentum :

$$\rho u \frac{\partial w}{\partial x} + \rho v \frac{\partial w}{\partial y} = \frac{\partial}{\partial y}\left(\mu \frac{\partial w}{\partial y}\right)$$

One should notice the analogy between this latter equation and the energy equation (Pr = 1).

$$\rho a \frac{\partial H}{\partial x} + \rho v \frac{\partial H}{\partial y} = \frac{\partial}{\partial y}\left(\mu \frac{\partial H}{\partial y}\right)$$

This, under adiabatic conditions has the trivial solution

$$H = He = Hw$$

Introducting the following notation :

$$\omega w = \frac{w_e}{\sqrt{2He}} = \text{constant}$$

$$\omega = \frac{\omega w^2}{1-\omega w^2}$$

$$K = \frac{w}{we}$$

and integrating the equations across the boundary layer, with the help of the Illingsworth-Stewartson transformation, one gets the following integral equations.

$$F \frac{d\delta_i^*}{dx} + \delta_i^* \left[\frac{\partial F}{\partial a}\frac{da}{dx} + \frac{\partial F}{\partial C}\frac{dc}{dx}\right] + f\delta_i^* \frac{d}{dx}\left(\ell n Me_\alpha\right) = \beta C_h \frac{M_{\infty\alpha}}{Me_\alpha} \frac{h}{Re_\alpha \delta_i^*}$$

$$H \frac{d\delta_i}{dx} + \delta_i^* \frac{dH}{ds}\frac{ds}{dx} + \delta_i^* \left(1+2H+\omega EPS\right) \frac{d}{dy}\left(\ell n Me_\alpha\right) = \beta C_h \frac{M_{\infty\alpha}}{M_{\infty\alpha}} \frac{P}{Re_\alpha \delta_i^*}$$

$$J \frac{d\delta_i^*}{dx} + \delta_i^* \frac{dJ}{da}\frac{da}{dx} + \delta_i^* \left(3J-2\omega TAU\right) \frac{d}{dx}\left(\ell n Me_\alpha\right) = \beta C_h \frac{M_{\infty\alpha}}{Me_\alpha} \frac{R}{Re_\alpha \delta_i^*}$$

$$Tw \frac{d\delta_i^*}{dx} + \delta_i^* \left[\frac{\partial Tw}{\partial a}\frac{da}{ax} + \frac{\partial Tw}{\partial c}\frac{dc}{dx}\right] + \delta_i Tw \frac{d}{dy}\left(\ell n Me\right) = \beta C_h \frac{M_{\infty\alpha}}{Me_\alpha} \frac{Qw}{Re_\alpha \delta_i^*}$$

Me_α and Re_α denote Mach and Reynolds number based on the external longitudinal velocity ue and u_∞. The quantities appearing in the equations are presented in Table 2. The integral quantities can be expressed as integrals of non dimensional longitudinal and transverse velocity profiles, for example

$$EPS = \alpha \int_0^n (1-K^2)\, dy$$

where

$$\alpha = \left[\int_0^n (1-f')dy\right]^{-1}$$

The identification parameters are :

$a = \eta\delta f''(0)$ for attached flow $\quad C = K'(0)$

$\frac{\eta f'=0}{\eta\delta}$ for separated flow

The velocity profiles (f' and K) are chosen to be the similar solutions of the boundary layer equations. They are thus the solutions of the Falkner Skan equations :

$$\begin{cases} f'''+ff''+\beta\left(1-f'^2+\omega(1-K^2)\right) = 0 \\ K''+fK' = 0 \end{cases}$$

with the boundary conditions

$\eta = 0$	$f = f' = 0$	$K = 0$
$\eta \to \infty$	$\lim_{\eta\to\infty} f' = 1$	$\lim_{\eta\to\infty} K = 1$

It can be noticed that the integral quantities do not depend explicitly on the parameter ω but only through the dependence on ω of the functions f and K. This dependence can be expected to be small and a unique representation for the integral quantities as a function of the identification parameters will be posible. This has been verified.

The coupling is given by a Prandtl Meyer relation in which all quantities are considered in the longitudinal plane.

$$\theta_e = tg^{-1}\frac{ve}{u_e} = \theta_0+\left[\sqrt{\frac{\gamma+1}{\gamma-1}}\,tg^{-1}\sqrt{\frac{\gamma-1}{\gamma+1}\,(M_\alpha^2-1)}-tg^{-1}\sqrt{M_\alpha^2-1}\right]$$

	y=	10		50		90		130	
	X_F	a	b	a	b	a	b	a	b
$\alpha=4°$	60	21.5	19	63	55	81.5	86	102.5	109
	90	27	25	55	60.5	113	79	141	113
	120	28	28	73	71	112	96	152	139
$\alpha=6°$	60	24	25	63.5	63.5	90.5	103.5	123	126.5
	90	26	24				95	137	120
$\alpha=8°$	60	24.5	23	60	65	94	98		
	90	26	26	67	71	104	102	128.5	120
	120	30	28	82	79	110	98	141	124.5

a : P = 11000 Pa

b : P = 22000 Pa

All distances in millimeters

TABLE 1 - UPSTREAM INFLUENCE

$$F = H + \frac{1+me_\alpha}{me_\alpha}\left\{1+\frac{\alpha_w{}^2}{1-\alpha_w{}^2}\overline{EPS}\right\} = H + \frac{1+me_\alpha}{me_\alpha}\left(1+\overline{EPS}\right)$$

$$f = \left\{2+\frac{\gamma+1}{\gamma-1}\frac{me_\alpha}{1+me_\alpha}\right\}H + \frac{3\gamma-1}{\gamma-1}\left(1+\overline{EPS}\right) + \left\{\frac{\gamma+1}{\gamma-1}\frac{1}{1+me_\alpha} - \frac{1}{me_\alpha}\right\}$$

$$h = \frac{M_e}{M_{\infty\alpha}}\frac{1+me_\alpha}{1+m_{\infty\alpha}}\frac{Re_j^*}{C_h}\frac{tg\varphi_e}{me_\alpha}$$

$$\beta = \frac{pea_e}{p_\infty a_\infty} = \left(\frac{1+m_e}{1+m_\infty}\right)^{-\frac{3\gamma-1}{2(\gamma-1)}} = \left(\frac{1+me_\alpha}{1+m_{\infty\alpha}}\right)^{-\frac{3\gamma-1}{2(\gamma-1)}}$$

$$m = \frac{\gamma-1}{2}M^2$$

$$\alpha = \left[\int_0^{\eta\delta}(1-f')d\eta\right]^{-1}$$

$$\overline{EPS} = \int_0^{\eta\delta}(1-K^2)d\eta$$

$$H = \alpha\int_0^{\eta\delta} f'(1-f')d\eta$$

$$\overline{TAU} = \alpha\int_0^{\eta\delta} f'(1-K^2)d\eta$$

$$J = \alpha\int_0^{\eta\delta} f'(1-f'^2)d\eta$$

$$z = \alpha\int_0^{\eta\delta} f'd\eta$$

$$\overline{T_w} = \alpha\int_0^{\eta\delta} f'(1-K)d\eta$$

$$P = \frac{f''(0)}{\alpha}$$

$$\overline{Q_w} = \frac{K'(0)}{\alpha}$$

$$R = \frac{2}{\alpha}\int_0^{\eta\delta} f''^2 d\eta$$

TABLE 2

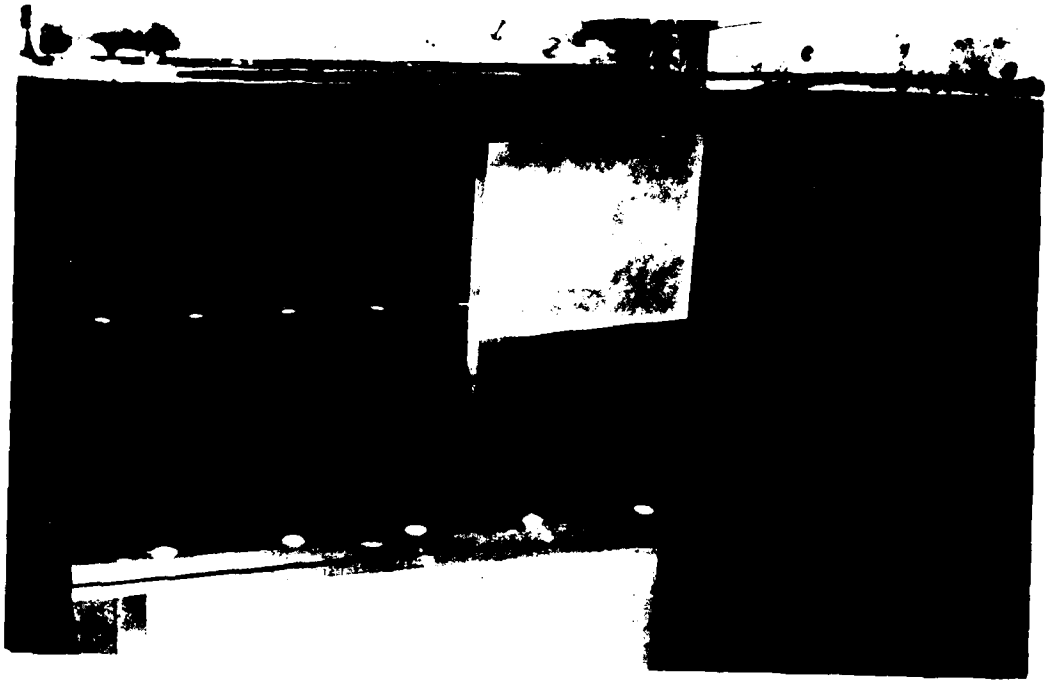

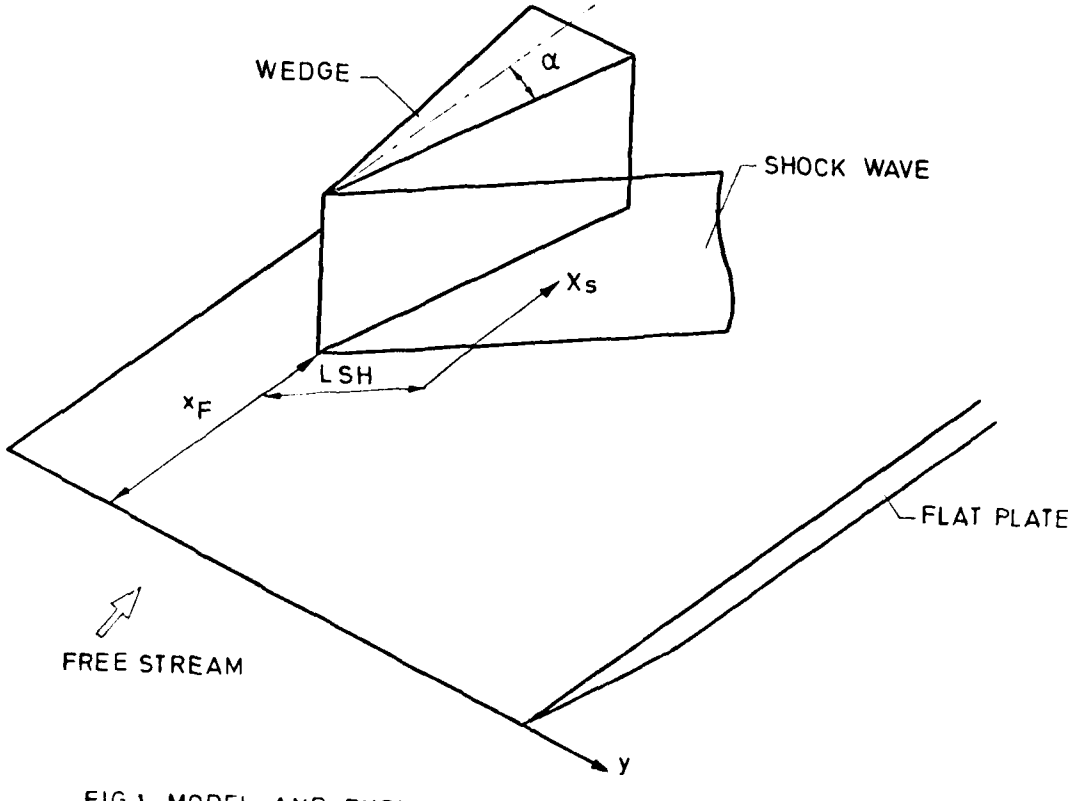

FIG.1-MODEL AND EXPERIMENTAL CONFIGURATION (IN REFLEXION FOR CLARITY)

FIG. 2 - DATA ACQUISITION SYSTEM.

FIG. 3 - MODEL INJECTED IN THE TUNNEL FOR SURFACE FLOW VISUALIZATION PHOTOGRAPHED AFTER A TEST.

FIG. 4 - SURFACE FLOW VISUALIZATION
$\alpha = 4°$, $X_F = 12$ cm, $Reu = 2.4\ 10^6/m$

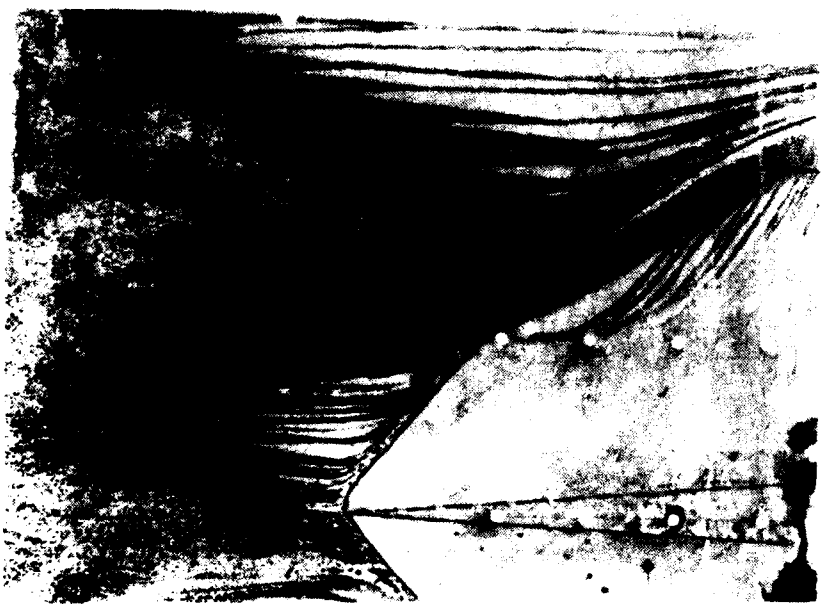

FIG. 5 - SURFACE FLOW VISUALIZATION
$\alpha = 6°$, $X_F = 12$ cm , $Re_u = 2.4\ 10^6/m$

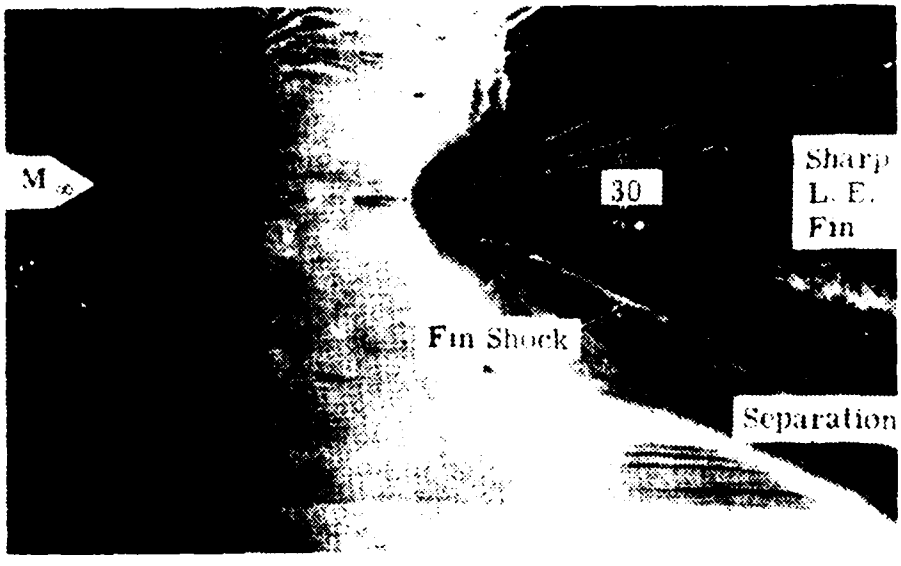

FIG. 6 - SURFACE FLOW VISUALIZATION OF A TRANSITIONAL INTERACTION (From ref. 2)

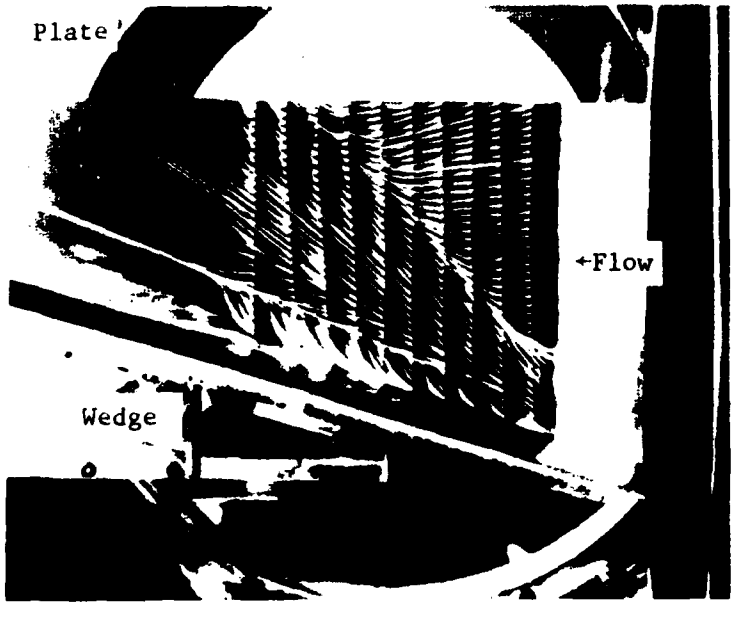

FIG. 7 - SURFACE FLOW VISUALIZATION IN THE CORNER OF TWO INTERSECTING WEDGES AT MACH 12.5 (From ref. 21)

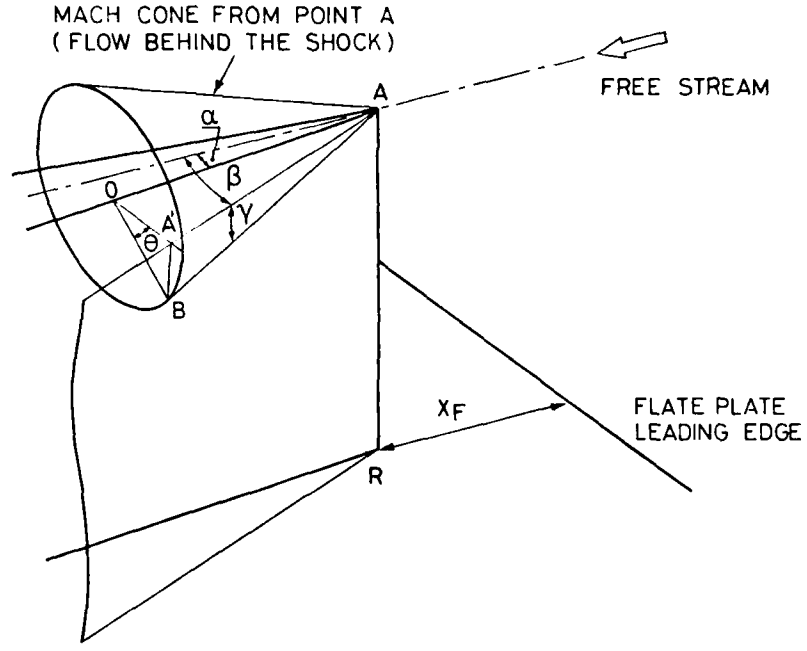

SHOCK WAVE (2 D OBLIQUE SHOCK THEORY)

NOTATIONS AND RELATIONS

α : WEDGE INCIDENCE.

β : SHOCK WAVE ANGLE.

M1 : MACH NUMBER IN THE FREE STREAM.

M2 : MACH NUMBER BEHIND OBLIQUE SHOCK.

$AO \equiv r$

$OA' = r\,tg(\beta - \alpha)$

$OB = r\,tg\,\mu_2$ WITH $\mu_2 = Sin^{-1}\left(\frac{1}{M_2}\right)$

$AA' = \frac{r}{\cos(\beta - \alpha)}$

$\longrightarrow \cos A = \frac{OA'}{OB} = \frac{tg(\beta - \alpha)}{tg\ \mu_2}$

$A'B = r\ tg\,\mu_2\ Sin\,\theta$

$tg\gamma = \frac{A'B}{AA'} = tg\,\mu_2\ Sin\,\theta \cos(\beta - \alpha)$

FIG. 8 - EXPERIMENTAL CONFIGURATION WITH SHOCK WAVE

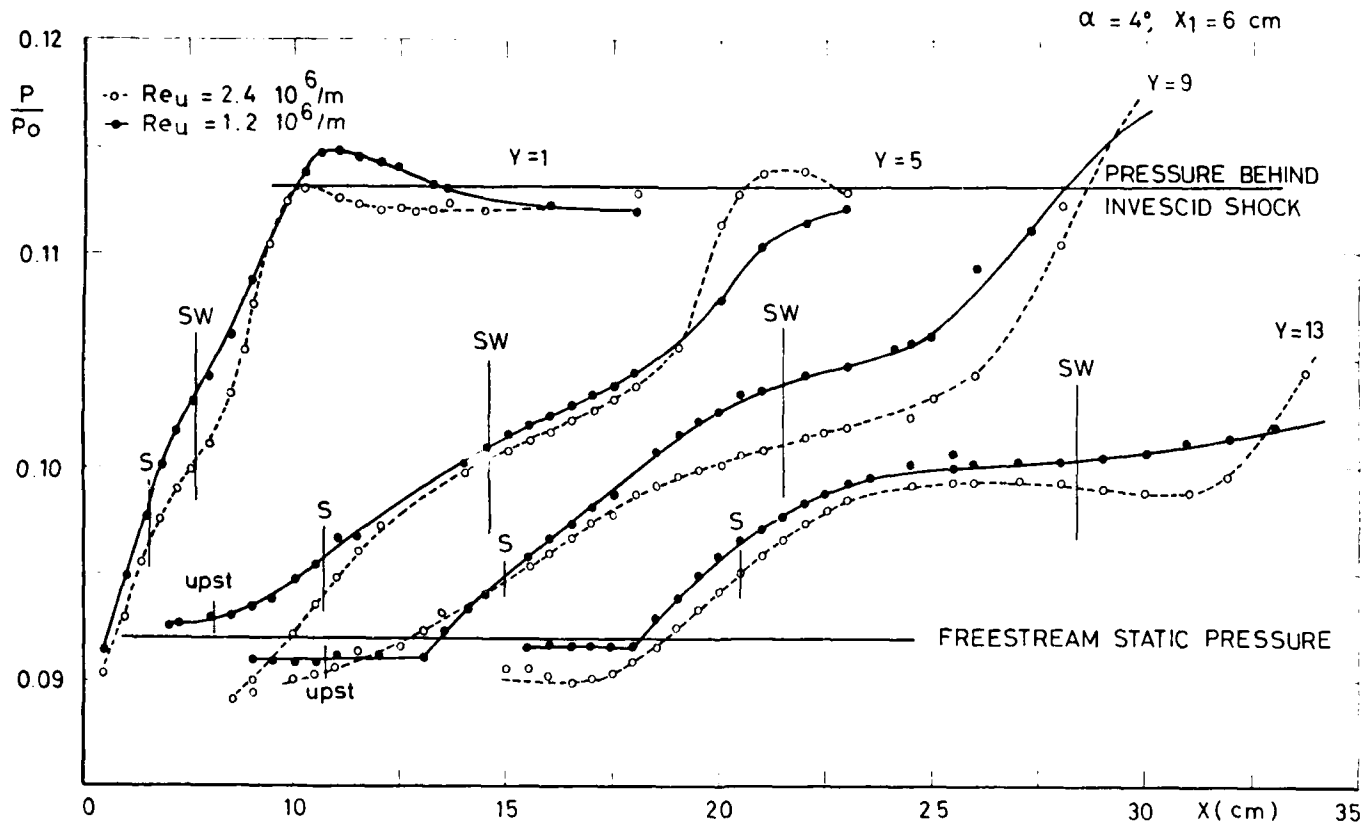

FIG. 9 - SURFACE PRESSURE DISTRIBUTIONS FOR DIFFERENT Y
SW : SHOCK WAVE LOCATION (FROM OBLIQUE SHOCK THEORY)
S : SEPARATION LINE LOCATION (FROM VISUALIZATIONS).

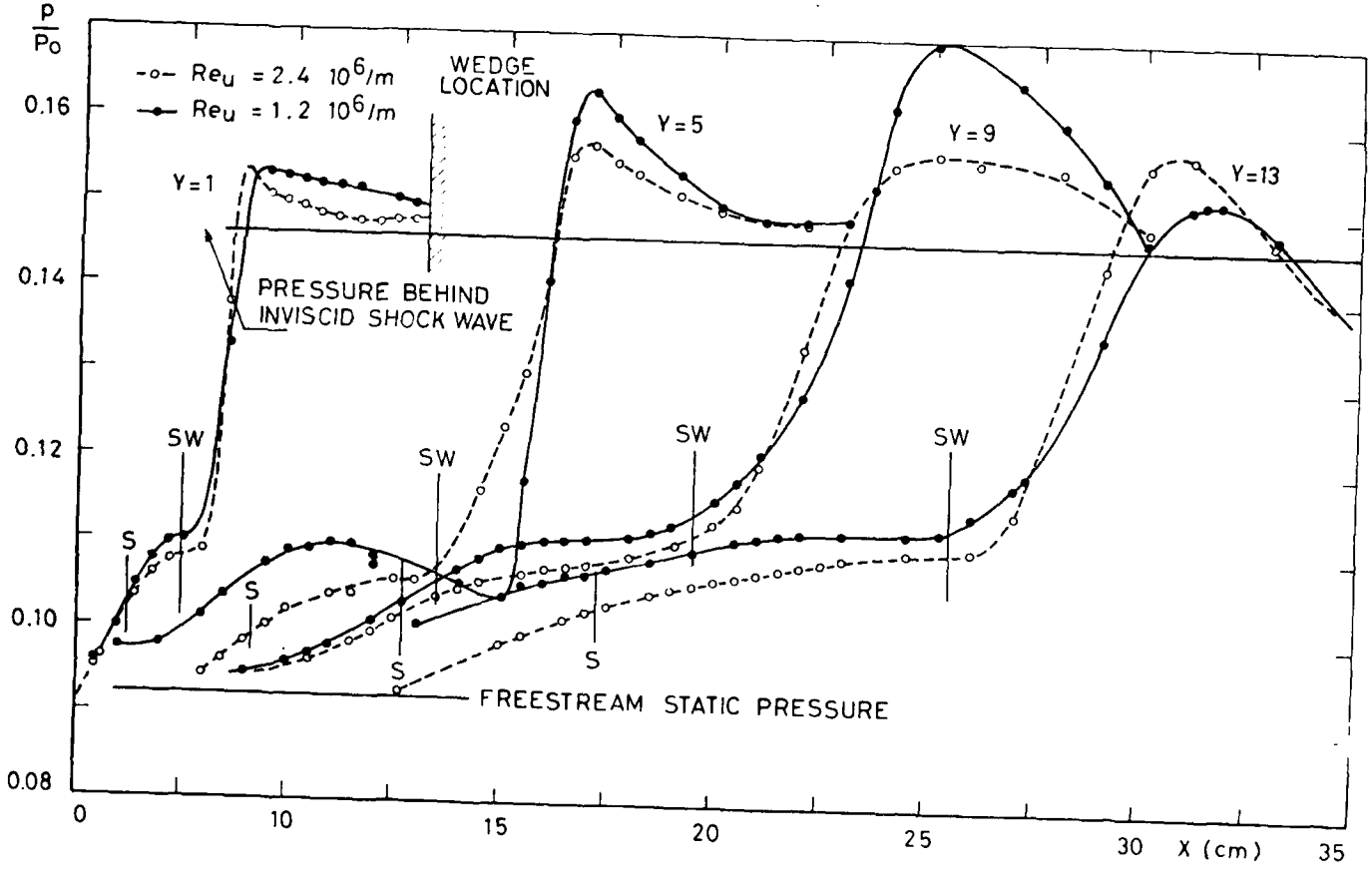

FIG. 11 - SURFACE PRESSURE DISTRIBUTIONS FOR DIFFERENT Y
SW : SHOCK WAVE LOCATION (FROM OBLIQUE SHOCK THEORY).
S : SEPARATION LINE LOCATION (FROM VISUALISATIONS)

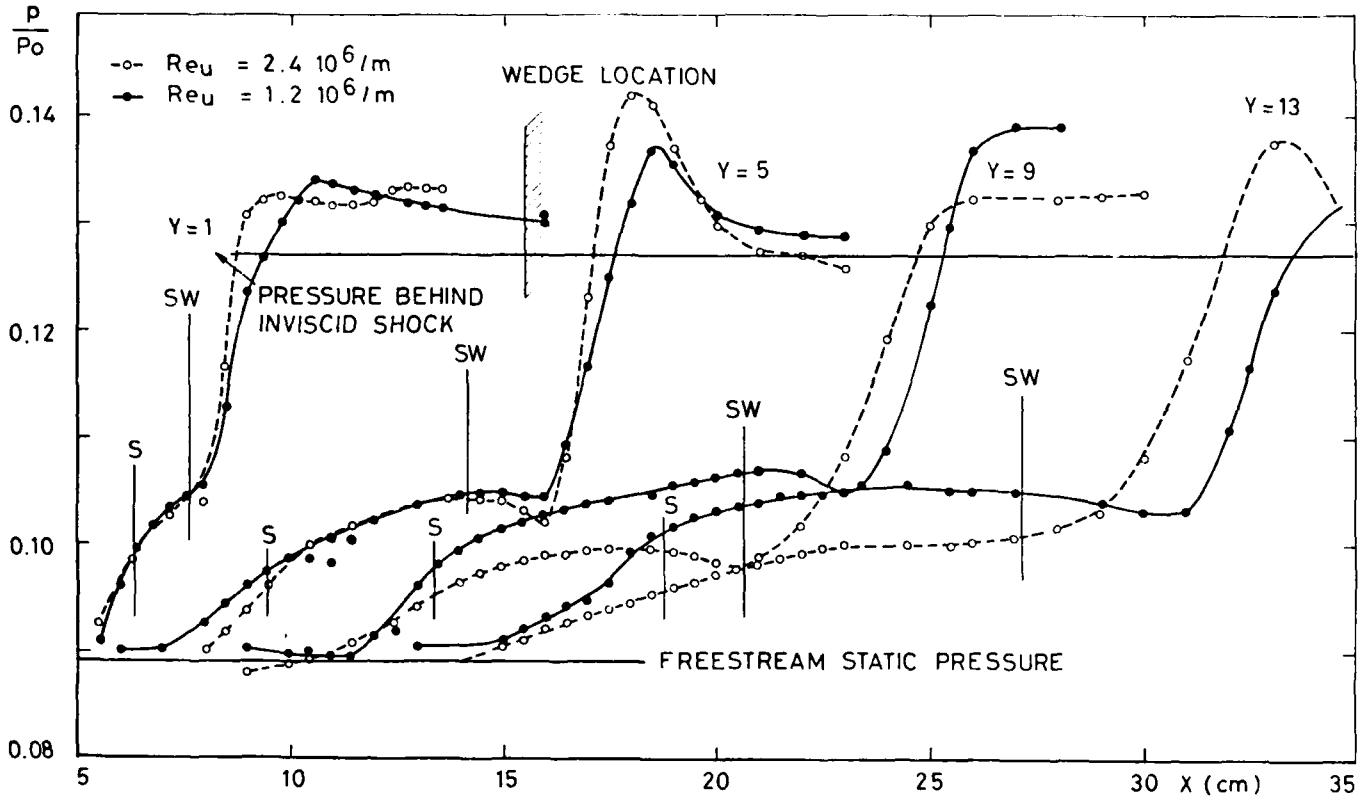

FIG. 10 - SURFACE PRESSURE DISTRIBUTIONS FOR DIFFERENT Y $\alpha = 6°$, $X_F = 6$ cm
SW : SHOCK WAVE LOCATION (FROM OBLIQUE SHOCK THEORY)
S : SEPARATION LINE LOCATION (FROM VISUALISATIONS)

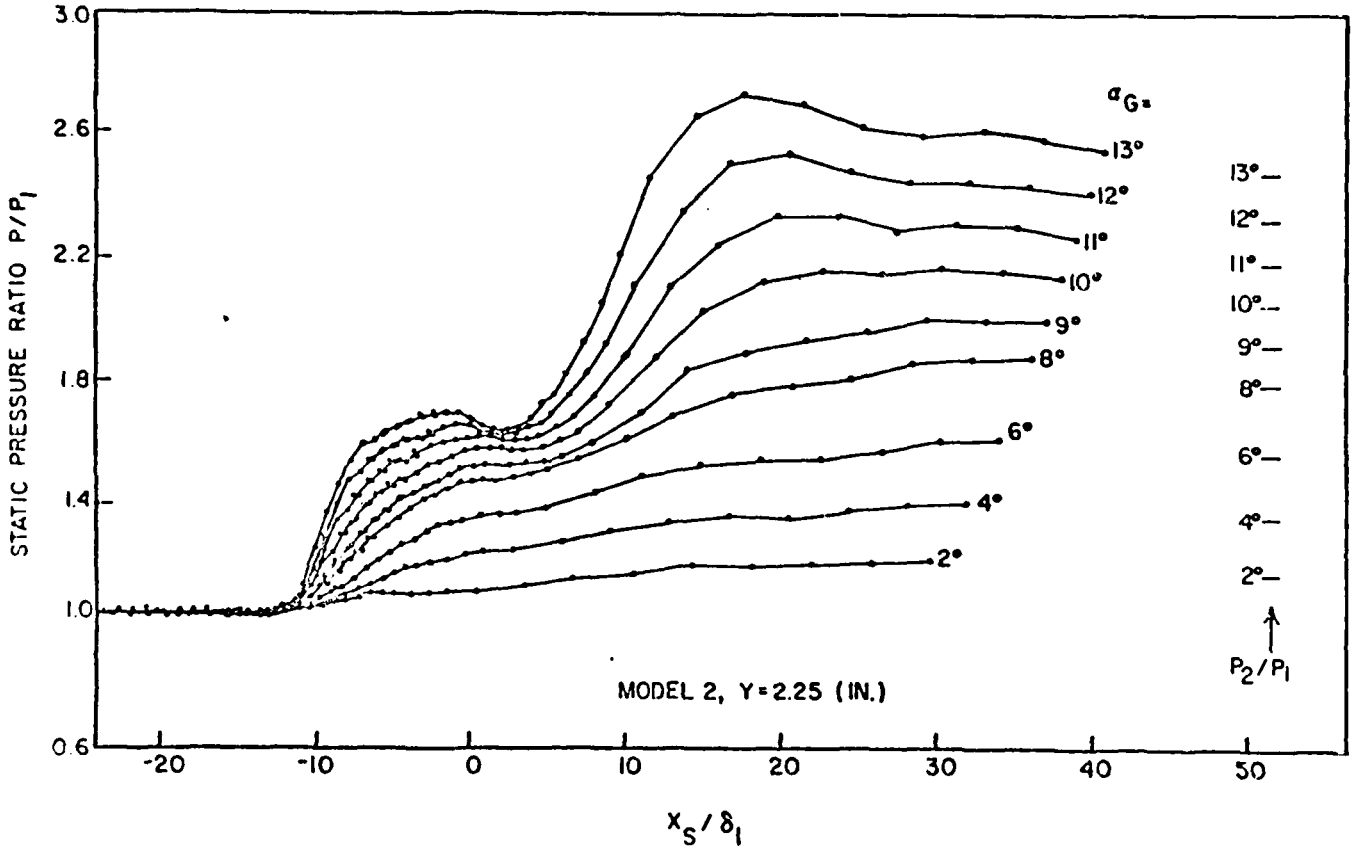

FIG. 12 - STATIC PRESSURE DISTRIBUTIONS, Y = 2.25 INCH , MODEL 2 (from ref. 6)

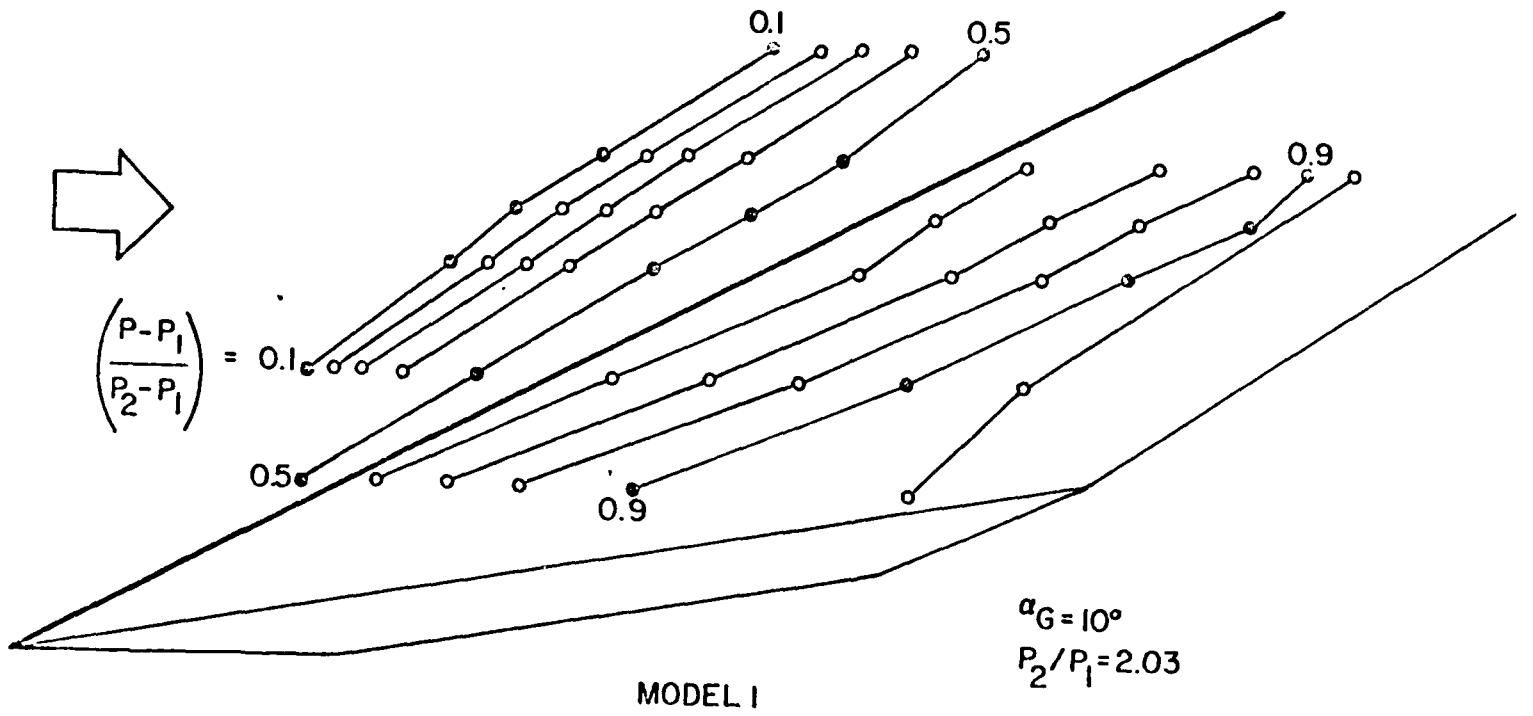

FIG. 13 - SURFACE ISOBAR PATTERN, α_G = 10°, MODEL 1, TUNNEL BOTTOMWALL
(from ref. 6)

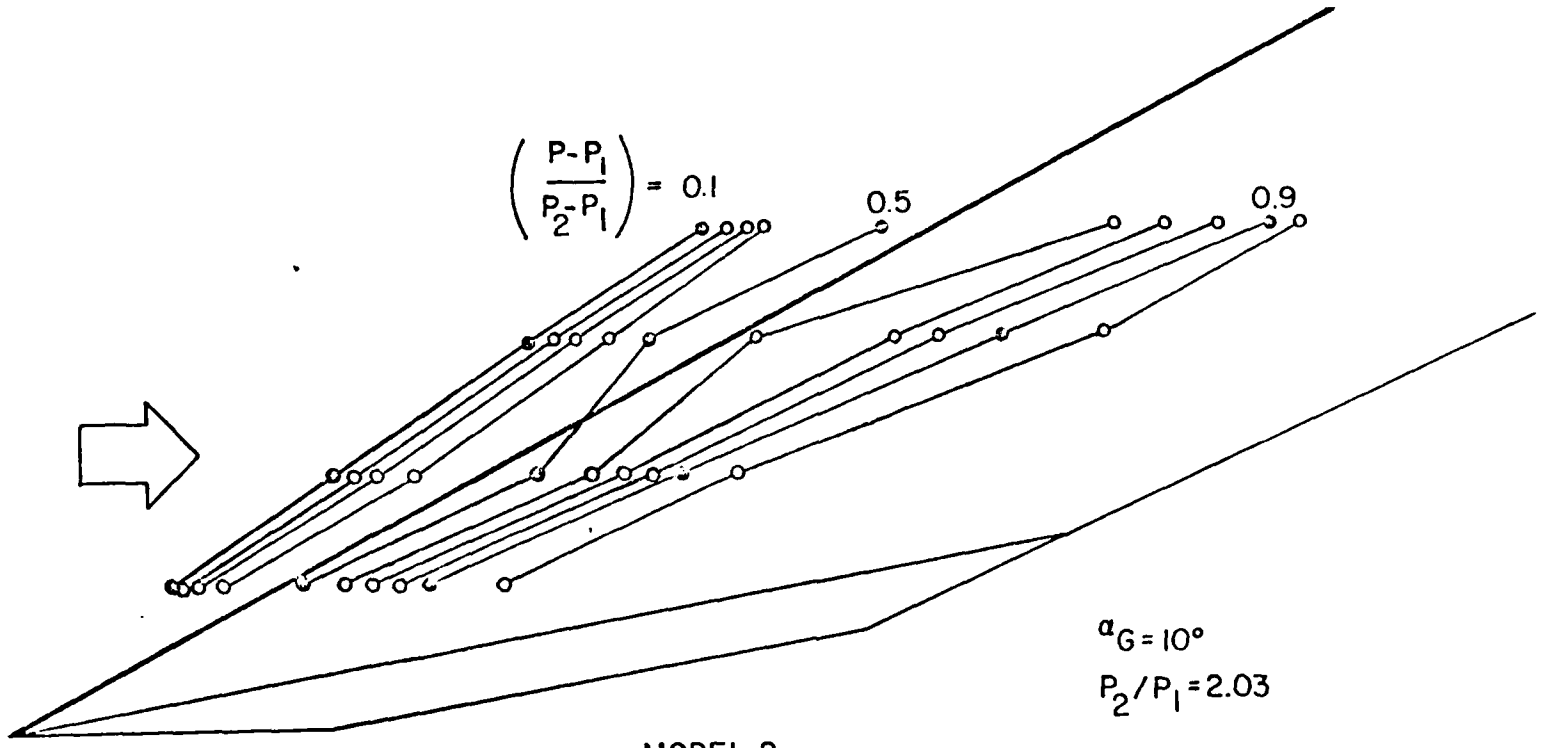

FIG. 14 - SURFACE ISOBAR PATTERN, $\alpha_G = 10°$, MODEL 2, FLAT PLATE SPANNING TUNNEL
(from ref. 6)

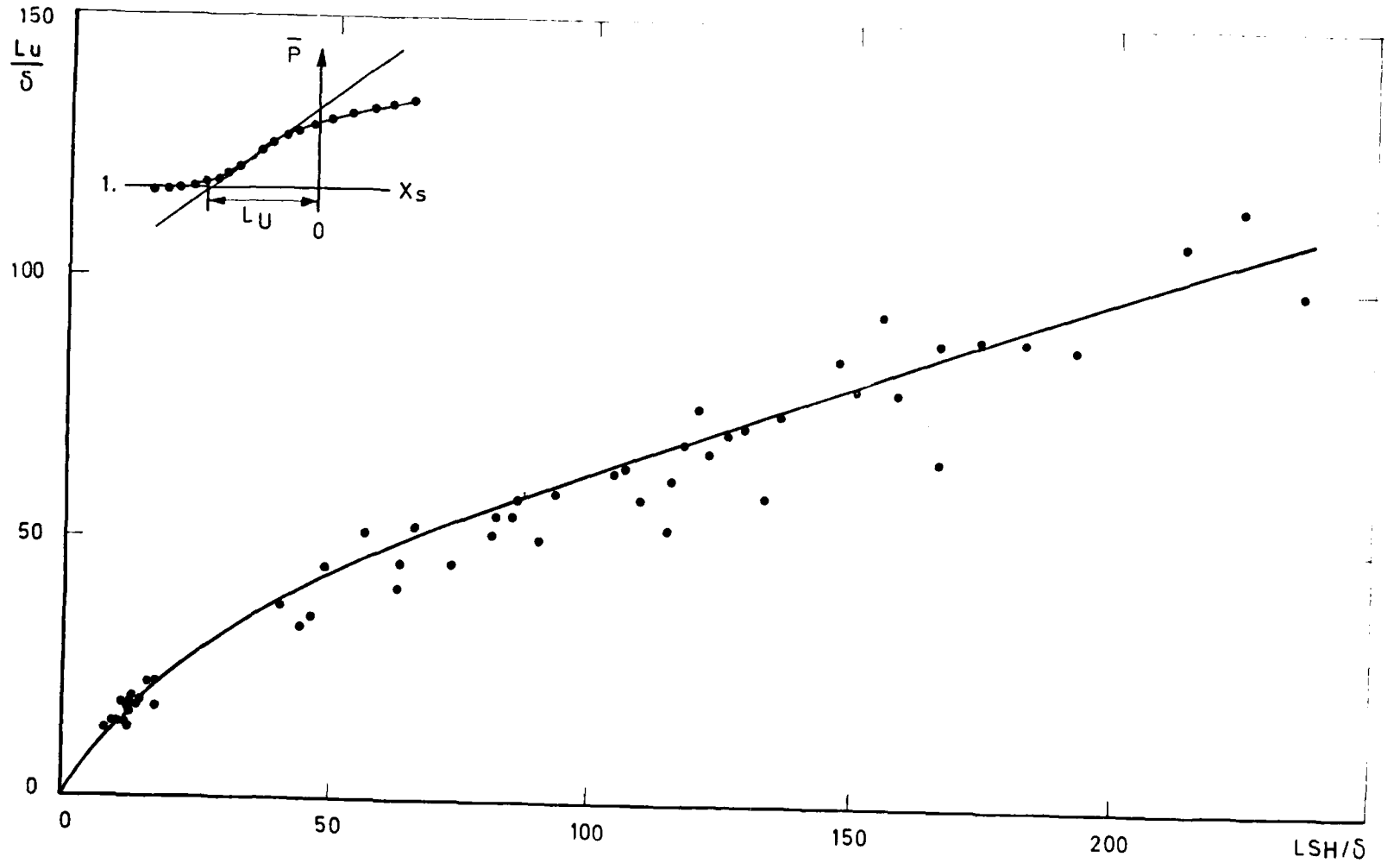

FIG. 15 - UPSTREAM INFLUENCE AS A FUNCTION OF DISTANCE FROM THE PIN

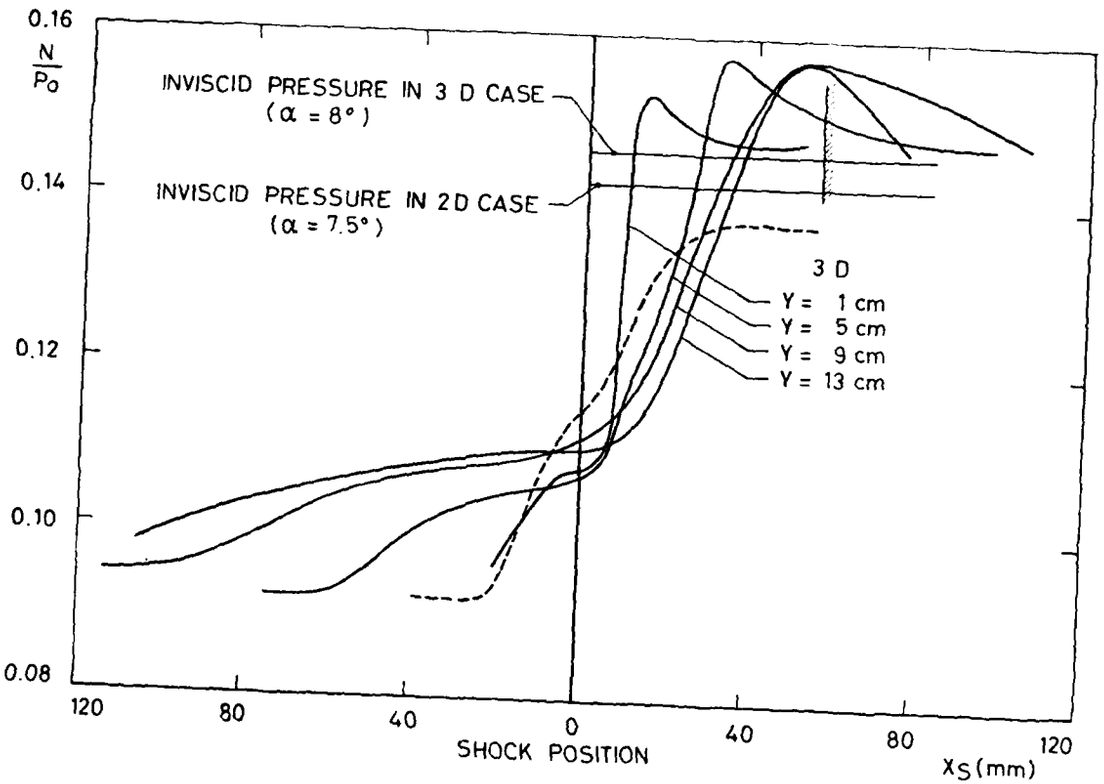

FIG. 16 - COMPARISON OF 2 D & 3D PRESSURE DISTRIBUTIONS

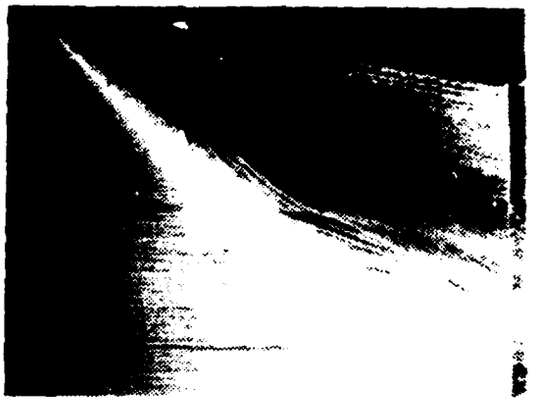

A $Re_l = 1.1 \times 10^6$

B $Re_l = 60 \times 10^6$

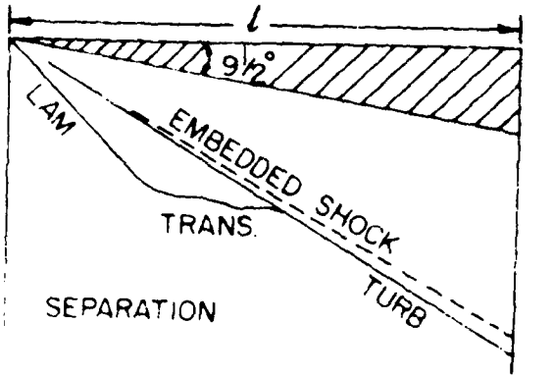

FIG. 17 - EFFECT OF TRANSITION ON SURFACE FLOW VISUALIZATION (From ref. 2)

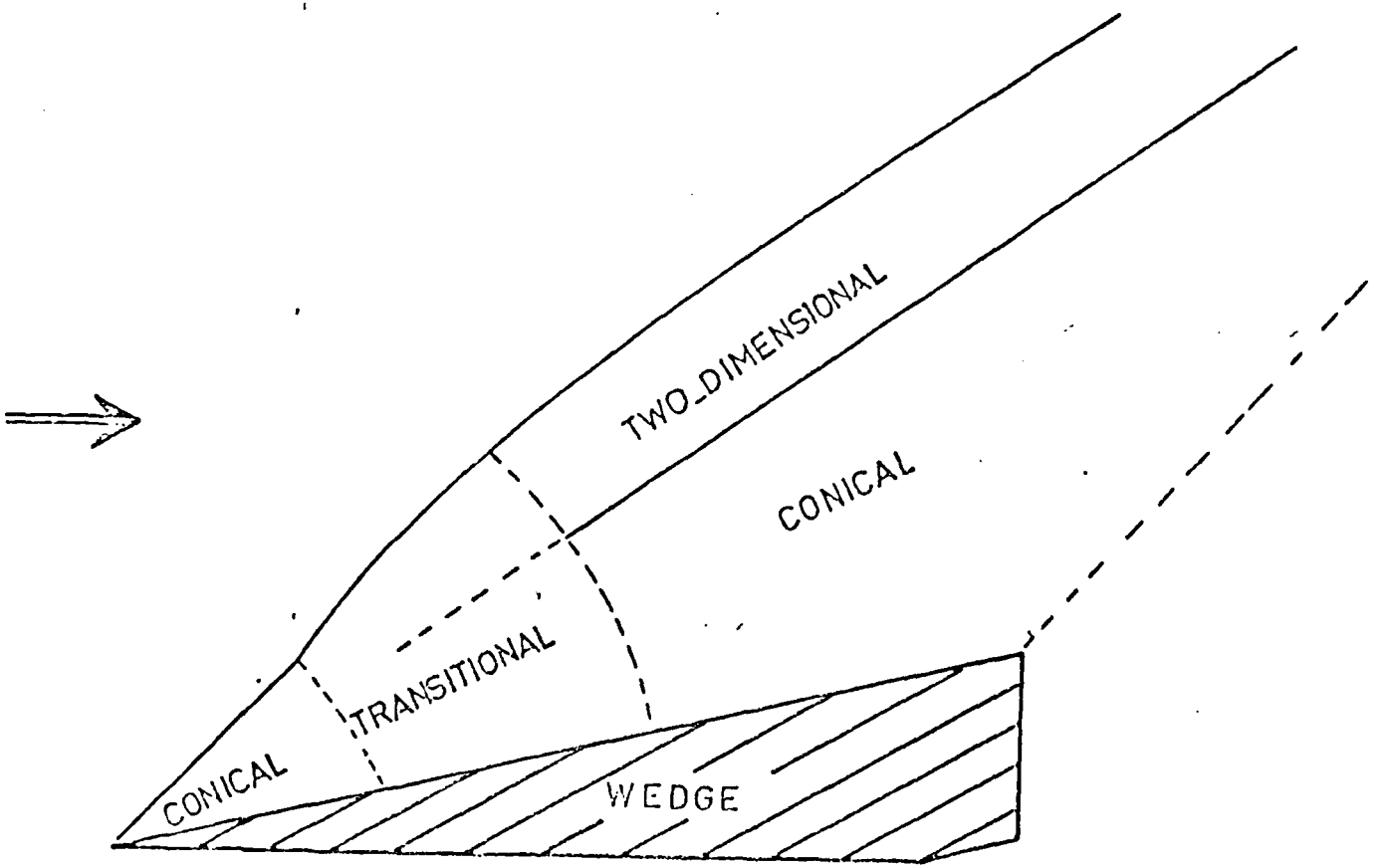

FLOW REGIONS FROM OIL FLOW MEASUREMENTS

FIG. 18 - DIFFERENT REGIONS IN A 3 D SKEWED SHOCK WAVE TURBULENT BOUNDARY LAYER INTERACTION (from ref. 30)

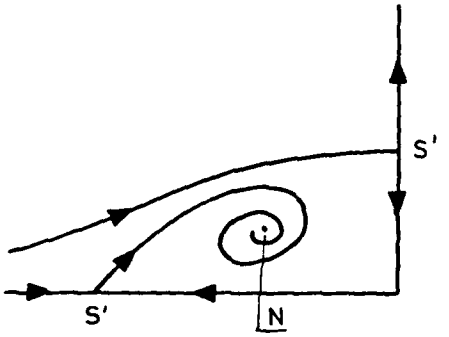

S' : SEMI-SADDLE POINT, N : FOCUS OR SPIRAL NODE
(NOTATIONS TAKEN FROM Ref. 17)

POSSIBLE FLOW PATTERN IN PLANE OF SYMMETRY
AHEAD OF A CYLINDRICAL PROTUBERANCE
(AFTER FLOW VISUALIZATIONS IN Ref. 35)

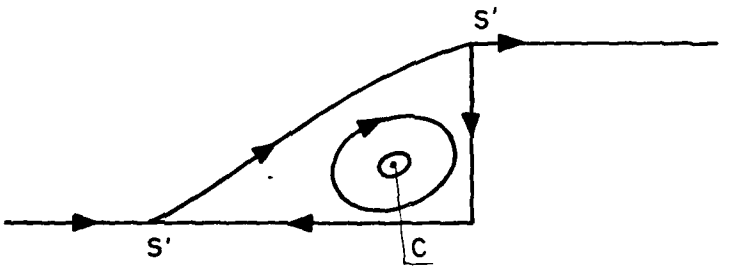

C : CENTRE

FLOW PATTERN AHEAD OF A 2D STEP

FIG. 19 - 3D & 2D SEPARATED PATTERNS.

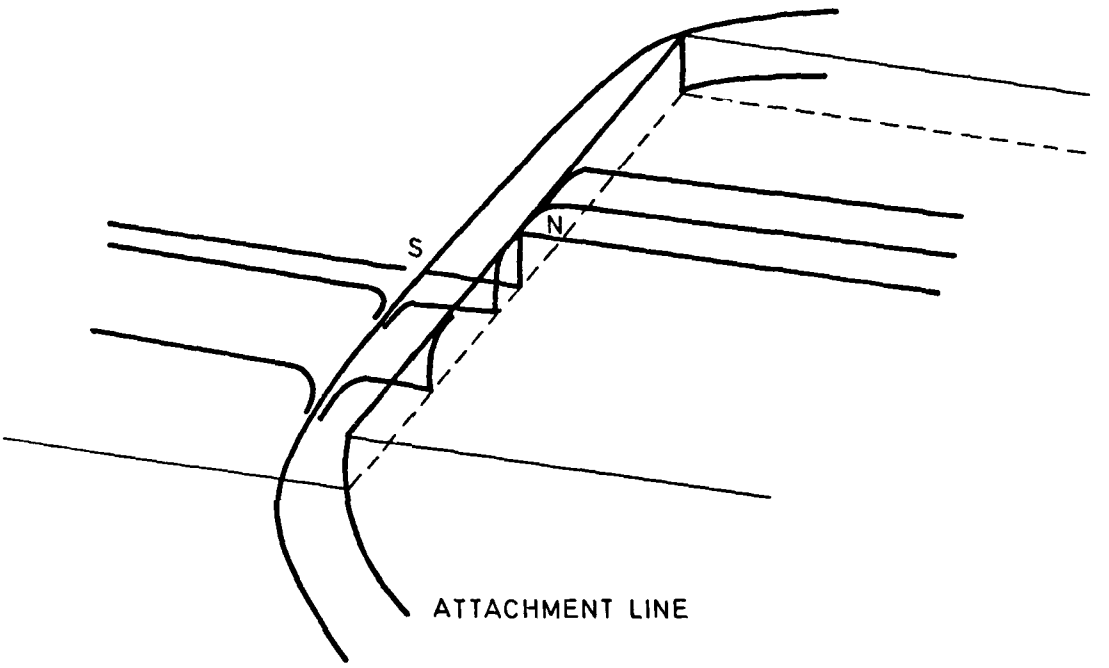

a) SURFACE FLOW PATTERN OF A LIMITE SIZE STEP WITH $\frac{L}{h} \gg 1$

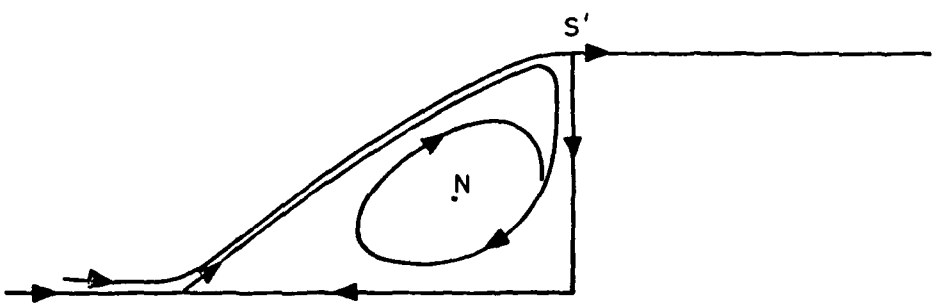

b) FLOW PATTERN IN THE CUT IN THE PLANE OF SYMMETRY

FIG. 20 - (QUASI 2 D) SEPARATED FLOW PATTERN

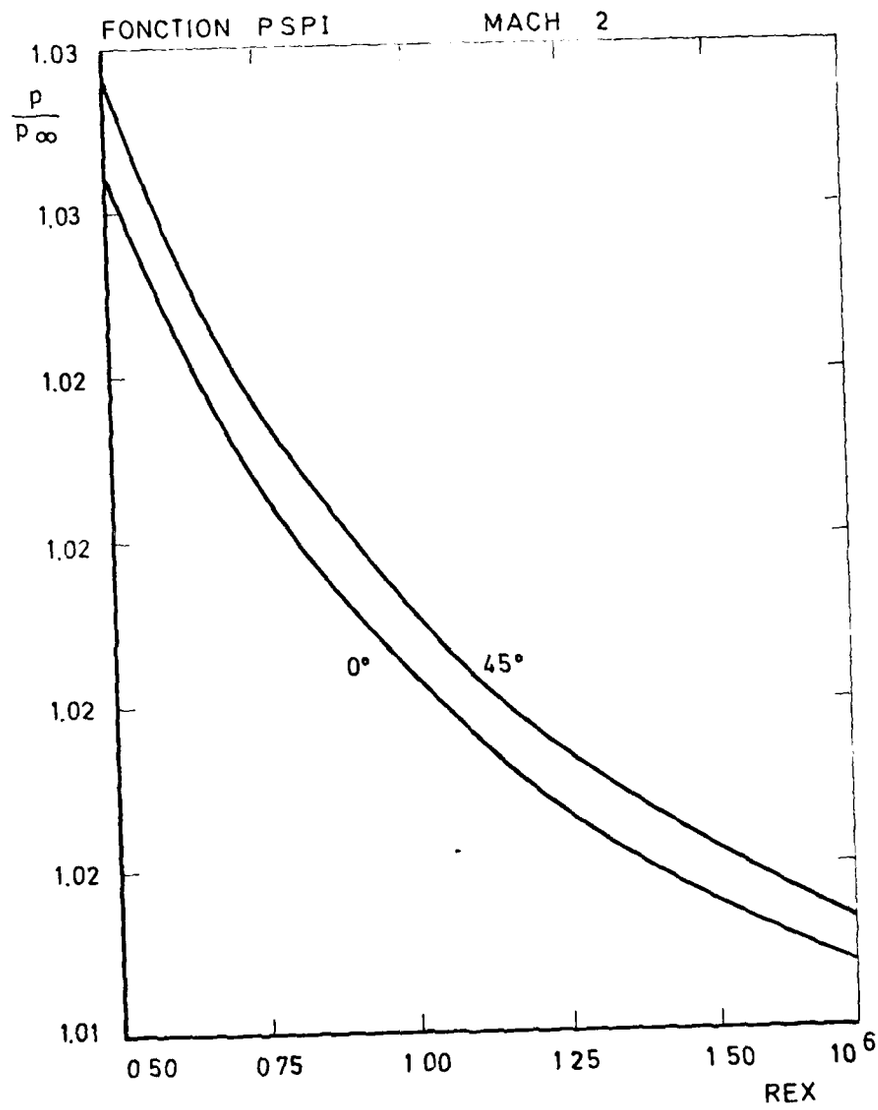

FIG. 21 - EFFECT OF SWEEP ON THE WEAK INTERACTION REGION

END

DATE
FILMED

2 - 84

DTIC